Journal Pre-proofs

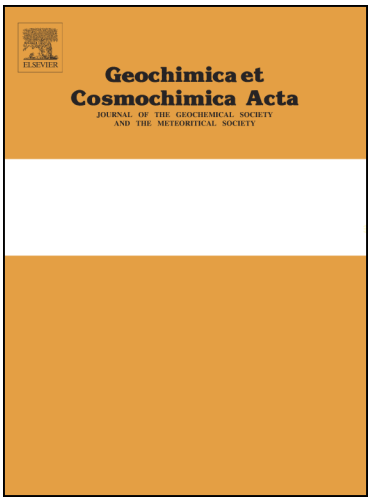

Platinum-group element geochemistry of the Paraná flood basalts – modelling metallogenesis in rifting continental plume environments

Jordan J. Lindsay, Jens C.Ø. Andersen, Hannah S.R. Hughes, Iain McDonald, Alan R. Hastie, Marcell L. Besser, Otavio A.B. Licht, Edir E. Arioli

PII: S0016-7037(21)00453-1
DOI: https://doi.org/10.1016/j.gca.2021.07.035
Reference: GCA 12319

To appear in: *Geochimica et Cosmochimica Acta*

Received Date: 17 December 2020
Revised Date: 24 July 2021
Accepted Date: 27 July 2021

Please cite this article as: Lindsay, J.J., Andersen, J.C., Hughes, H.S.R., McDonald, I., Hastie, A.R., Besser, M.L., Licht, O.A.B., Arioli, E.E., Platinum-group element geochemistry of the Paraná flood basalts – modelling metallogenesis in rifting continental plume environments, *Geochimica et Cosmochimica Acta* (2021), doi: https://doi.org/10.1016/j.gca.2021.07.035

Platinum-group element geochemistry of the Paraná flood basalts – modelling metallogenesis in rifting continental plume environments

Jordan J. Lindsay [a†], Jens C. Ø. Andersen [a], Hannah S. R. Hughes [a], Iain McDonald [b], Alan R. Hastie [c], Marcell L. Besser [d], Otavio A. B. Licht [e], Edir E. Arioli [f]

[a] Camborne School of Mines, University of Exeter, Penryn Campus, Penryn, Cornwall, TR10 9FE, United Kingdom

[b] School of Earth and Ocean Sciences, Main College, Cardiff University, Park Place, Cardiff, CF10 3AT, United Kingdom

[c] School of Geoscience, University of Edinburgh, Drummond Street, Edinburgh, EH8 9XP, United Kingdom

[d] Serviço Geológico do Paraná (State of Paraná Geological Survey), Curitiba, Paraná, Brazil

[e] Setor de Ciências da Terra, Universidade Federal do Paraná (UFPR), Curitiba, Paraná, Brazil

[f] Instituto de Terras Cartografia e Geologia, Governo do Paraná, Curitiba, Paraná, Brazil

† Corresponding author: e-mail, jordan@minviro.com

Abstract

The 135 Ma Paraná-Etendeka Large Igneous Province (PELIP) is one of the largest areas of continental flood basalt (CFB) volcanism in the world and is widely agreed to be a product of intracontinental melts related to thermal anomalies from the Tristan mantle plume. The province rifted during the break-up of Gondwana, as the plume transitioned into an oceanic geodynamic environment. This study reports analyses of plume-derived basalts from the Brazilian side of the PELIP (the Serra Geral Group) to investigate major, trace and platinum-group element (PGE) abundances in an evolving plume-rift metallogenic setting, with the aim of contextualising metallogenic controls alongside existing magmatic interpretations of the region. The chalcophile geochemistry of these basalts defines three distinct metallogenic groupings that fit with three modern multi-element magma classifications for Serra Geral lavas. In this scheme, *Type 4* lavas have a distinctive PGE-poor signature, *Type 1 (Central-Northern)* lavas are enriched in Pd, Au and Cu, and *Type 1 (Southern)* lavas are enriched in Ru and Rh. Our trace element melt modelling indicates that the compositional variations result from changes in the melting regime between the garnet and spinel stability fields, in response to the thinning and 'unlidding' of the rifting continent above. This process imposes progressively shallower melting depths and higher degrees of partial melting. Accordingly, *Type 4* magmas formed from small degree melts, reducing the likelihood of sulfide exhaustion/chalcophile acquisition at source. *Type 1 (Central-Northern)* magmas incorporated components of the sub-continental lithospheric mantle (SCLM)-derived in higher-degree partial melts; the SCLM was heterogeneously enriched via metasomatism prior to plume melting, and this produced enrichment in volatile metals (Pd, Cu, and Au) in these magmas. In contrast, the Ru-Rh enrichment in *Type 1 (Southern)* lavas is attributed to increased spinel-group mineral *and* sulphide incorporation from the mantle into higher degree partial melts close to the continental rift zone. Our models confirm the importance of contributions from SCLM melts in precious metal mineral systems within CFB provinces, and reinforce the role of heterogeneous metasomatic enrichment underneath cratons in boosting intracontinental prospectivity with respect to ore deposits.

1. Introduction

1.1. Mantle Plumes and Precious Metals

Many of the world's important magmatic sulphide deposits are found within continental flood basalt (CFB) provinces (e.g. Lightfoot et al., 1993; Naldrett, 1997). Whereas the mineralisation processes at work in each CFB are primarily controlled by mid- to upper-crustal differentiation mechanisms (e.g. Thompson and Gibson, 1991; Ellam, 1992; Maier and Groves, 2011), the initial geochemical fingerprint of CFB magmas can have important implications for metallogenic fertility and understanding how metals are mobilised from the mantle (e.g. Hawkesworth et al., 1988; Wooden et al., 1993; Wilson et al., 1996; Bierlein et al., 2009).

Localities with prominent PGE orthomagmatic sulphide deposits share a similar geodynamic setting, with plume-derived (i.e. intraplate) magmas interacting with thick continental cratons and their margins. Plumes represent buoyant material from mantle discontinuities that rise to the base of the crust (e.g. Morgan, 1971; Morgan, 1972; Shannon and Agee, 1998; Jellinek and Manga, 2004; Burke et al., 2008; Deschamps et al., 2011; Li and Zhong, 2017), inducing partial melting and magma generation in the asthenosphere and lowermost lithosphere (Jerram and Widdowson, 2005 and references therein). Decompression models for CFB melting predict ~5 % of the lithosphere (particularly the sub-continental lithospheric mantle or SCLM) is involved in melt generation, and this contribution is dominant in the early stages of rifting (e.g. McKenzie and White, 1989; White and McKenzie, 1995; Turner et al., 1996; Howarth and Harris, 2017). An observed spatial association between PGE-rich ore deposits and Archaean lithosphere may indicate that the 'inheritance' of precious metals play an important role in dictating aspects of the geochemistry of plume-derived magmas and mineralisation (e.g. Downes, 2001; Hawkesworth and Scherstén, 2007; Zhang et al., 2008; Maier and Groves, 2011; Maier et al., 2012; Griffin et al., 2013; Barnes et al., 2015).

Here, we examine the nature of the interactions between plumes and the SCLM and their role as a control on PGE (and other metal) content of CFB parental magmas. Work on the North Atlantic Igneous

Province (NAIP) demonstrates that plume environments that transition from continental to oceanic settings, as well as changes in the thickness and nature of lithosphere above the region of partial melting, directly affect the PGE geochemistry of ascending plume-derived magmas (e.g. Andersen et al., 2002; Hughes et al., 2015). Continental lavas from Greenland and the British Isles exhibit distinctly higher Pt/Pd ratios than oceanic lavas from Iceland, attributed to a shifting "metal basket" (i.e. the concentration and variety of precious and/or base metals) and variable SCLM incorporation in partial melts (Hughes et al., 2015). In this study, we investigate lavas associated with the Tristan plume and the Paraná-Etendeka Large Igneous Province (PELIP) in the South Atlantic in order to test how (if) the PGE, Au and base metal geochemistry of the CFB province changed through time and space. The PELIP shares a similar transitional continent-to-ocean geodynamic setting to the NAIP. If the inherent controls of trace element and isotopic variation in regional magmas reflect distinct geodynamic controls, this should be evident in PGE and other chalcophile elements. New geochemical data for onshore South American PELIP flood basalts are compared and used in quantitative geochemical melt modelling, to assess how PGE geochemistry changes through the evolution of the CFB province, with a focus on the link between variable SCLM properties and resulting partial melt compositions.

1.2. Formation of the Paraná-Etendeka Large Igneous Province (PELIP)

Currently positioned in the centre of the southern Atlantic Ocean, the Tristan plume has migrated through a cratonic, to continental margin, to mid-oceanic setting throughout the Cretaceous and Cenozoic (Fodor and Vetter, 1984). It is active today under the islands of Tristan da Cunha and Gough, but has a >130 million year history of volcanism that spans two continents and the entire width of the South Atlantic (Stewart et al., 1996). The plume head stage is thought to be responsible for the eruption of the PELIP, one of the largest CFB provinces in the world (Courtillot et al., 2003), in addition to the Rio Grande Rise and Walvis Ridge topographic features on the ocean floor (e.g. Camboa and Rabinowitz, 1984; O'Connor and Duncan, 1990; Ussami et al., 2013) (Fig. 1a). The Tristan plume is one of the world's "primary hotspots" according to Courtillot et al. (2003), satisfying the criteria of creating

linear chains of age-progressive volcanics, exhibiting large flood basalt buoyancy flux, high $^{3}He/^{4}He$ isotope ratios and significant low shear wave velocity anomalies in the mantle below.

The ~1.7 million km^3 PELIP is spread asymmetrically between (primarily) Paraná, Brazil and Etendeka, Namibia (which were conjoined in the Cretaceous; Fig. 1a), with fifteen times higher volume of lavas found in South America than Africa (Fodor et al., 1989). Intraplate magmas are typically chemically variable and are derived from relatively undepleted mantle (e.g. Zindler and Hart, 1986; Stracke et al., 2005; Hawkesworth and Scherstén, 2007). The Tristan plume arrived at the Gondwanan lithosphere under the modern day central Paraná region in Brazil at ca. 135 Ma, inducing partial melting in the asthenosphere (Stewart et al., 1996). The duration of eruption of the onshore PELIP has been debated, ranging from <1 million years (suggesting a high eruption rate of around 1.5 km^3/year; Renne et al., 1996) to 10 million years (suggesting a much lower eruption rate of under 0.1 km^3/year; Stewart et al., 1996). Recent studies suggest a conservative 0.8 km^3/year for the majority of the flood eruption (Beccaluva et al., 2020), comparable to other CFB provinces, such as those that produced the Deccan and Karoo traps (Natali et al., 2017 and references therein). The PELIP eruption rate is broadly similar to the NAIP (a mean of 0.6 km^3/year; Eldholm and Grue, 1994).

From 134 to 128 Ma (Stewart et al., 1996), rifting initiated in the thermally thinned Gondwanan continental lithosphere (e.g. McKenzie and White, 1989; Turner et al., 1996; de Wit et al., 2008). North-westerly plate movement migrated plume activity to the Etendeka-Angola margin, synchronous with the eruption of the south-eastern lavas in Paraná (Beccaluva et al., 2020) (Fig 1b). Following significant extension and basin formation as the South American and African continents drifted apart (Martins-Ferreira et al., 2020 and references therein), the asthenosphere above the Tristan plume continued to undergo partial melting and eruption of lava on the seafloor throughout the Cretaceous. Sustained volcanism formed ridges on either side of the mid-oceanic rift, the Rio Grande Rise (west) and the Walvis Ridge (east) that connect the PELIP to the modern active hotspot islands of Tristan da Cunha and Gough (e.g. O'Connor and Duncan, 1990; O'Connor and Jokat, 2015; Homrighausen et al.,

2019). Figure 1b summarises the different chemostratigraphic stages of PELIP magmatism with respect to congruent rifting.

1.3. Geochemical classification of the Paraná flood basalts

The South American portion of the PELIP erupted over the Botucatu Sandstones and Proterozoic basement of the Paraná Basin. The basin is oriented NE-SW with its morphology controlled by three major underlying structures – the Ponta Grossa and Rio Grande arcs, and the Torres Trough (e.g. Cordani and Vandoros, 1967; Peate et al., 1992; Besser et al., 2018). On average, the basin-filling lavas in the region are >1 km thick, with thicknesses of up to 1.7 km towards the north (Gordon, 1947; Leinz, 1949; Leinz et al., 1966; Peate et al., 1990). The Paraná lavas, referred to more formally as the Serra Geral Group in Brazil (e.g. Licht, 2018; Rossetti et al., 2018), are primarily basaltic to basaltic-andesitic and compositionally grouped into synchronous High-Ti (HT) in north-central Paraná and Low-Ti (LT) in the south-east. The HT and LT lavas often inter-finger in central Paraná due to their synchronous eruptive sequence (e.g. Licht, 2018). Volcanism in the southeast laterally evolved into bimodal mafic-felsic volcanism, producing significant amounts of silicic lavas (e.g. Peate et al., 1992; Polo et al., 2018).

Given that the Serra Geral lavas are thought to have erupted simultaneously throughout the province via different melting sources rather than by differentiation processes from a single source (Peate, 1997), the underlying stratigraphy of the Paraná Basin is complex (Turner et al., 1999; Rossetti et al., 2018). Recent studies suggest that the synchronous HT and LT lavas were erupted from separate sub-surface magma plumbing systems spawned from plume-derived melting, and followed separate magmatic differentiation routes and localised melting processes (Natali et al., 2016; Licht, 2018), with rare evidence for minor interaction between HT and LT magmas in plumbing systems (De Min et al., 2017). LT magmas reflect higher degrees of crustal contamination in contrast to limited (or absent) crustal contamination for the HT magmas (e.g. Piccirillo et al., 1988; Peate et al., 1992; Peate and Hawkesworth, 1996; Turner et al., 1996; Rocha-Júnior et al., 2013; Natali et al., 2017; Marques et al., 2018).

Whereas the mafic Serra Geral lavas are similar in both hand specimen and thin section, the magma-types exhibit small differences in modal mineralogy and larger differences bulk geochemical compositions. Consequently, pioneering studies on the geochemistry of the Serra Geral Group further classified the HT, LT and silicic magma-types based on major and trace element, and isotopic variations (e.g. Bellieni et al., 1984; Fodor, 1987; Peate et al., 1992; Peate, 1997). With time, increasingly more sophisticated distinctions across multi-element parameters have been sought (e.g., the sixteen Si-Ti-Zr-P divisions introduced by Licht, 2018). A generalised northern and southern stratigraphy for Serra Geral is given in Figure 1c, and Table 1 compares the Peate et al (1992) and Licht (2018) classifications, with an indication of Si, Zr, Ti and P concentration cut-offs for the latter. In this paper, we address the intersection between geochemical characteristics of both naming schemes, with particular emphasis on PGE concentrations.

1.3.1.High-Ti Group

The HT basalts are classified into three major magma-types – Paranapanema, Pitanga and Urubici. Pitanga and Urubici lavas have the highest TiO_2 concentrations (>3 wt.%) (Peate et al., 1992). Pitanga and Paranapanema are found exposed almost exclusively in central-northern Paraná, while Urubici outcrops primarily intercalated with Gramado (of the LT lavas) (Fig. 1c) (Peate et al., 1999). Paranapanema lavas belong to the HT group despite having a lower TiO_2 concentration than the other two HT members (between Esmeralda and Pitanga at 1.7-3.2 wt.%; Peate, 1997) and being found throughout the region. Urubici is significantly enriched in light rare earth elements (LREE) and high field strength elements (HFS) in comparison to the other HT magma-types (Peate et al., 1999). Pitanga is generally slightly more enriched than Paranapanema in most trace elements, excluding the transition metals Ni, Co, Cr and Sc (Rocha-Júnior et al., 2013). Despite major and trace element differences, the three magma-types have similar isotopic signatures (with $(^{87}Sr/^{86}Sr)_i$ ratios of 0.7048 to 0.7065 and εNd of -1 to -4; Peate and Hawkesworth, 1996). This led to them being grouped together as the "northern basalts" in many early Sr-Nd-Pb isotope studies (e.g. Richardson et al., 1982; Peate

et al., 1992; Peate and Hawkesworth, 1996). Licht (2018) classifies Urubici and Pitanga as Type 4 (>2.85 wt.% TiO_2) and Paranapanema as Type 1 (Central-Northern) (<2.85 wt.% TiO_2), a significant distinction from classic studies (Table 1).

Paranapanema and Pitanga each contribute to 20 % of the total Serra Geral volume, and Urubici contributes ~5 %. Urubici lavas are the most sparsely observed at surface, although it is seen in the highlands of São Joaquim and as sills interbedded with Vale do Sol in the south-east of the CFB province (Besser et al., 2018). Paranapanema overlies Pitanga throughout most of the flood sequence; however it underlies Gramado in the very south of the basin (Bellieni et al., 1984).

1.3.2. Low-Ti Group

The LT basalts to basaltic-andesites (Gramado, Esmeralda and Ribeira) comprise around 50 % of the total eruptive volume of the Serra Geral Group and are found in the south of the CFB province (Peate, 1997). Over a third of the total lava volume belongs to the Gramado magma-type, and 5-10 % to the Esmeralda magma-type (Peate et al., 1992). As per Peate (1997), both magma-types see distinctive enrichment of heavy rare earth elements (HREE) and large-ion lithophile (LIL) elements relative to HFS elements and LREE, and a negative Ti anomaly when normalised against mantle compositions. Esmeralda has highly variable εNd (-4 to 4), while maintaining consistent initial Sr isotope values ($(^{87}Sr/^{86}Sr)_I$ = 0.7046-0.7086) (Peate and Hawkesworth, 1996. Gramado lavas have the lowest TiO_2 (as low as 0.7 wt.%) and εNd (-9 to -4) in the Serra Geral sequence, with higher and much more varied ($^{87}Sr/^{86}Sr)_i$ ratios (0.7075-0.7167) relative to Esmeralda, which sets it apart from all other mafic lavas in the Serra Geral Group (Peate and Hawkesworth, 1996). The Gramado magma-type is considered to be formed from the most crustally-contaminated Tristan plume-derived magmas. In the southern Paraná Basin, Gramado is normally found on the flanks of the inland Serra Geral escarpment and at the coast near Torres, whilst Esmeralda is found on the flatter plateau tops. This reflects their general relative positioning within the lava pile as per Figure 1c (Peate, 1997). Recent studies have further subdivided Gramado into the Torres and Vale do Sol Formations in the modern framework (Rossetti

et al., 2018 and references therein). The Gramado and Esmeralda magma-types comprise the Type 1 (Southern) classification from Licht (2018) (<2.85 wt.% $TiO_{2;}$ Table 1).

Rarely found exposed at the surface (i.e., sampled primarily via drilling), the LT Ribeira lavas have low TiO_2 concentrations, but slightly higher Ti/Y than Gramado and Esmeralda (Ti/Y ration has occasionally been used in place of TiO_2 as a more specialised LT/HT group discriminator - Peate et al., 1992; Peate and Hawkesworth, 1996). In contrast, the LT Ribeira $(^{87}Sr/^{86}Sr)_i$ signature is more in line with HT magma-types (0.7055-0.7060 compared to 0.7046-0.7167 for LT; Peate et al., 1992), but lacks the accompanying HFS and LREE enrichment expected of the HT group. Despite having more in common geochemically with the LT group, the transitional Ribeira lavas are found interbedded with HT lavas in the northern zone (Peate et al., 1992), essentially an intermediate lava overlapping the geochemical properties of both HT and LT magma-types (Fig. 1c).

1.3.3. Silicic Group

Mafic lavas in central and southern Paraná are often associated with the silicic lavas of the Chapecó and Palmas magma-types, predominantly within the bimodality of south-eastern LT group (Fig. 1c) (e.g. Bellieni et al., 1984; Peate et al., 1990; Peate et al., 1992; Garland et al., 1995; Peate, 1997). Chapecó lavas are higher in TiO_2 than Palmas, and their relative geographic location mimics that of the mafic HT/LT split, placing Chapecó further northwest than its counterpart. The rhyolites, dacites and related alkali complexes of Paraná have been dated to co-exist with the pre-rift stages of flood basalt volcanism, which further reinforces the complexity of the multi-source melting beneath the province – the silicic lavas are likely derived from mid- to upper-crustal differentiation processes from the source of flood basalt volcanism (e.g. Milner et al., 1995). The Serra Geral silicic rocks have been interpreted to be genetically related to their mafic equivalents via fractional crystallisation – Chapecó represents partial melt extraction in HT basalts in the lower crust whilst Palmas represents the differentiation of LT basalts in the upper crust (Garland et al., 1995). Licht (2018) provided distinctions for eight high-Si magma-types with varying Zr, TiO_2 and P_2O_5 concentrations – Palmas fits within Type

9 and Chapecó within Type 14, and they contribute to around 20 % of samples classified in the region (Table 1). However, as silicic rocks are very rarely associated with PGE mineralisation, the focus of our paper lies on the mafic magma-types whilst using these more evolved compositions as reference material for geochemical trends.

2. Materials and Methods

2.1. Sample acquisition

We present a new suite of major, trace and PGE analyses for 85 basalt and 7 rhyolite samples from the Serra Geral Group. Samples were collected during two field expeditions, one in the north (focusing on HT lavas of Paraná State) and one in the south (focusing on LT and Silicic groups of the Santa Catarina and Rio Grande do Sul States). Figure 1c shows the general sample localities within the context of the Paraná Basin, with reference to underlying lava group. A complete sample database with field descriptions is provided in Supplementary A1.

2.2. Laboratory techniques

Weathered material and amygdales were removed from all samples prior to preparation, as these would interfere with primary geochemical concentrations. Rock samples were crushed to 1-2 mm chips using a jaw crusher before being milled in a chrome-steel TEMA mill to produce fine powders, which were used in all subsequent bulk geochemical analyses.

Major element oxides were measured using X-ray fluorescence (XRF) (after Kystol and Larsen, 1999; Tegner et al., 2009) at Camborne School of Mines, University of Exeter. Dried and ignited samples were fused in a furnace in platinum crucibles with lithium borate flux. Ammonium iodide solution was added to the molten sample to act as a wetting agent when poured into moulds. Cooled samples were analysed at 50-111 mA and 27-60 kV using a Bruker S4 Pioneer XRF spectrometer. Concentrations

were corrected to anhydrous values. The AGV-1, BHVO-2, BIR and DNC-1 standards were used in analyses and reported alongside new data.

Trace elements were measured using inductively coupled plasma mass spectrometry (ICP-MS) (after McDonald and Viljoen, 2006), also at Camborne School of Mines. Powdered samples were dissolved using 4-Acid digestion technique (nitric, perchloric, hydrofluoric and hydrochloric acids), and elemental concentrations were detected by an Agilent 7700 Series mass spectrometer. The BCR-2 and Bir-1a standards were used in analyses and reported alongside new data.

Six PGE (Os, Ir, Ru, Rh, Pt, Pd) plus Au were measured using Ni-S fire assay followed by tellurium co-precipitation and ICP-MS analysis at Cardiff University (using methods developed by Huber et al., 2001; McDonald and Viljoen, 2006). Fifteen gram aliquots of each powdered sample was mixed with 12 g of borax flux, 6 g $NaCO_3$, 0.9 g solid sulfur, 1.08 g Ni and 1 g silica, before being melted in a furnace at 1000°C for 1.5 hours. The sulfide bead separated from the cooled melt was removed, dissolved in hydrochloric acid, co-precipitated with Te, filtered and diluted before element detection using a mass spectrometer. It should be noted Os was not measured for the northern sample set due to the lack of volatilisation-free methods at the time of analyses; samples analysed at a later date were measured for Os given the advancement of methodological accuracy. The TBD1 and WPR1 standards were used in analyses and reported alongside new data. Detection limits (i.e., lowest recorded blank values) were 0.0052 ppb for Os, 0.0026 ppb for Ir, 0.0603 ppb for Ru, 0.0152 ppb for Rh, 0.1458 ppb for Pt, 0.0662 ppb for Pd and 0.0070 ppb for Au.

Full raw major, trace and PGE-Au data, plus standard measurements for each method (plus published values) and detection limits for PGE and Au are provided in Supplementary B. An amalgamated data sheet with duplicate measurements is available in Supplementary C. We acknowledge that chrome-steel mills can introduce small amounts of metal contamination to samples and although this is expected to be minimal and non-intrusive to our results (Evans et al., 2013), we have supplied quartz

sand procedural blank measurements for PGE analyses alongside Supplementary B, processed identically to our basalts.

2.3. Petrology of Samples

In general, basalts from each magma-type are aphyric/fine- to medium-grained with small phenocrysts of pyroxene or plagioclase (up to 1 mm), and are exceptionally fresh for lavas of their age (alteration information in Supplementary D). In thin section, olivine is notably sparse or absent in most mafic rocks, with orthopyroxene (normative 10-30 wt.%), clinopyroxene (normative 5-40 wt.%), plagioclase (normative 20-50 wt.%), and spinel-group minerals (normative 1-5 wt.%) dominating in the majority of samples. Silicic rocks (rhyolites to dacites; Fig. 2) are fine grain-sized, with plagioclase (20-30 wt.%), clinopyroxene (~10 wt.%) and magnetite (1-5 wt.%) phenocrysts, in a plagioclase-quartz-K-feldspar groundmass. Volcanic glass and quartz-feldspar aggregates (spherulites) are common throughout. Chapecó samples have larger and more frequent plagioclase phenocrysts than Palmas. There are no visible sulphides in any of our Serra Geral hand specimens, but rare traces (<1 wt.%, <0.1 mm crystals) can be found in thin sections.

We have used a combination of two classification schemes alongside sampling locations in order to utilise the wealth of literature already available describing the characteristics of lavas belonging to each magma-type. In this way, we can contextualise subtleties in the dataset according to PGE and Au and therefore metallogenic processes in the new precious metal data set. Accordingly, lava samples have been classified into their classic magma-types (except Ribeira, which was not sampled) based on bulk concentrations of MgO and TiO_2, plus Ti/Y and Ti/Zr ratios (established by Peate et al., 1992) and MgO vs. Zr, with literature data used for comparison (Fig. 2a-c; Supplementary A2). Classifications from Licht (2018) are also given for each sample (denoted by symbology), based on Si, Ti, Zr and P concentrations. The inherent issue with classifying samples based on limited bivariate relationships is evident – samples SG11-12, SG56 and SG78-79 do not conform to the Peate et al. (1992) classification

for example, and thus their designation was assessed subjectively based on adjacent literature data clouds for the purpose of this study; Licht (2018) classifications are wider, but more robust.

The sample set is also classified using a total alkali vs. silica (TAS) plot in Figure 2d. The mafic samples are predominantly basalts to basaltic andesites, with some Gramado samples classifying as andesites. Palmas samples plots within the dacitic field, while the two Chapecó samples plot with trachytes. All Paraná lavas analysed fall within the sub-alkaline to transitional alkali-tholeiitic fields.

3. Results

3.1. Major and trace element geochemistry

3.1.1. Major element oxides

Serra Geral basalts tend to have MgO concentrations consistently between 2 and 7 wt.%; silicic lavas plot between 1 and 2 wt.% MgO. Concentrations of TiO_2 highlight the established literature magma-types – >3 wt.% for Urubici/Pitanga or Type 4, 1.5-2.5 wt.% for Paranapanema or Type 1 (Central-Northern), and <1.5 wt.% for Gramado/Esmeralda or Type 1 (Southern), plus the silicic lavas (Fig. 3a). All basic lavas exhibit Fe_2O_3 between 10 and 16 wt.% (Fig. 3b), with HT samples generally higher than LT. In Figure 3c, LT lavas exhibit higher Al_2O_3 concentrations than HT lavas (the opposite to Fe_2O_3), with a slightly positive relationship with MgO; MnO concentrations follow this same slight positive relationship but between 0.15 and 0.35 wt.% (Fig. 3d). A distinctly positive correlation between MgO and CaO (Fig. 3e), and negative correlations between MgO and Na_2O (Fig. 3f), and MgO and K_2O (Fig. 3g) do not show clear HT-LT distribution patterns. Finally, P_2O_5 exhibits a bifurcated negative trend with MgO, with a shallow slope for LT and silicic lavas, and a steeper slope for HT lavas excluding Paranapanema, which follow LT trends (Fig. 3h).

3.1.2. Base metals

Trends in base metal enrichment are limited for the Serra Geral data set, with distinctively low overall Ni (<140 ppm; Fig. 4a) and Cr (<160 ppm; Fig. 4d) contents compared to other CFB provinces (e.g., the

NAIP where onshore lavas generally exhibit Ni concentrations of 100-1,000 ppm and Cr concentrations of 100-2,000 ppm; Hughes et al., 2015). The Paranapanema samples display positive correlations between MgO and Ni, Co and Cr concentrations (Fig. 4a, 4c, 4d) that have a similar slope but higher concentrations than Gramado and Esmeralda samples; Urubici and Pitanga samples lack strong trends in all instances. Enrichment of Ni, Cr and Co (Fig. 4c) follow very similar trends to Fe_2O_3 relative to MgO (Fig. 3b), with HT lavas generally containing slightly higher concentrations. Overall, Cu concentrations are better clustered into locality classifications than Ni, Cr or Co, with Paranapanema lavas exhibiting the highest mean Cu content at 254 ppm and Esmeralda exhibiting the highest single-sample concentrations (Fig. 4b). Unlike the Ni and Cr, concentrations of Cu and Co (Fig. 4b and 4c) are comparable to NAIP onshore lavas from Hughes et al. (2015), at around 10-500 ppm for Cu and 10-70 ppm for Co.

3.1.3. Rare earth elements and lithophiles

Chondrite-normalised (McDonough and Sun, 1995) REE plots for all Serra Geral magma-types have fractionated REE patterns, with LREE > HREE in all samples (Figs. 5a-f). Steeper gradients are observed in the HT lavas (Figs. 5a-c), with distinctive light REE enrichment especially in Urubici (Fig. 5a) and Pitanga (Fig. 5b); these two magma-types also exhibit parallel arrays, and all HT lavas have a narrower spread of concentrations. Paranapanema lavas (Fig. 5c) feature similar enrichment patterns to the LT group, not their designated HT group. The LT REE arrays (Figs. 5d-e) have more variable LREE concentrations than HT lavas, particularly in the more incompatible REE such as La, Ce, Pr, Nd and Sm. Esmeralda is the most depleted magma-type in all element concentrations (Fig. 5d). Silicic and LT lavas have prominent Eu troughs, with the Silicic group generally showing more enriched concentrations of all elements, particularly Chapecó (Fig. 5f).

Although some Gramado lavas trend towards high SiO_2 concentrations and progressively lower Nb/La ratios associated with vectors indicating assimilation and fractional crystallisation (AFC) in CFB magmas, the majority of Paraná samples do not share this trend (plots taken from Xiao et al., 2004)

(Fig. 6a). Most HT lavas are associated with OIB $(Th/Ta)_n$, $(Sm/Yb)_n$ and $(La/Sm)_n$ vectors, whilst LT lavas trend towards classic Low-Ti signatures found in Gondwana CFBs (Wooden et al., 1993) (Figs. 6b-c). Paranapanema, Gramado and Esmeralda magma-types, or Type 1 from Licht (2018) (Table 1), share a strong association in Figures 6b and 6d at $(Sm/Yb)_n$ ~2. Urubici and Pitanga lavas (i.e. Type 4 in Licht, 2018) trend together towards higher $(Sm/Yb_)_n$ >3.

The three HT magma-types exhibit similar normalised incompatible element patterns to one another and are enriched in Ba, Nd, Hf and Zr, and depleted in Sr and P compared to the LT samples (Fig. 7a-c). Esmeralda (Fig. 7d) and Gramado (Fig. 7e) samples exhibit a wide range of multi-element normalised signatures, primarily lower than all other magma-types, with Ba, Nb, Sr, P and Ti negative anomalies and depletions in the most incompatible elements including Hf, Zr, Sm and Tb in particular. Chapecó and Palmas have similar normalised incompatible element enrichment trends, with pronounced Nb, Sr and Ti negative anomalies, and high Rb, Th, U, K, Hf and Zr concentrations (Fig. 7f). Chapecó features slightly higher concentrations overall and a positive Ba anomaly, whilst Palmas features a negative one.

3.2. PGE and Au

Chondrite-normalised PGE and Au plots (McDonough and Sun, 1995) demonstrate a relative enrichment of Pd-group PGE (PPGE; Rh, Pt, Pd) and Au compared to Ir-group PGE (IPGE; Os, Ir, Ru) in all Serra Geral magma-types (except Palmas, which was not analysed) (Figs. 8a-f). However, the degree of enrichment varies significantly across the sample set. This is most obvious between Serra Geral HT and LT groups, with HT exhibiting a steep slope from IPGE to PPGE (Figs. 8a-c) and the LT showing normalised IPGE concentrations up to an order of magnitude higher than HT samples, producing a flatter gradient into PPGE (Fig. 8d-e). Most importantly, Serra Geral LT samples, or Type 1 (Southern) samples, frequently display an unusual, distinctive 'hump' between Ru, Rh and Pt concentrations and significant Pt, Pd and Au depletions compared to the gradual slope seen in the HT plot (with particularly high Pd and Au). Paranapanema lavas, or Type 1 Central-Northern, have the highest Pd

concentrations as shown by up to 0.1 x chondritic values (compared to 0.001-0.01 x chondrite for other lavas) in Figure 8c.

The highest concentrations of Ir, Ru and Rh (Fig. 9b-d) are found in LT rocks (around 1.2, 13.5 and 5.75 ppb, respectively), while Pt is most enriched in LT and Paranapanema (up to 30-40 ppb; Fig. 9e). Paranapanema lavas are distinctly Pd-rich in most instances (ranging 5-35 ppb compared to 1-15 ppb in all other lavas; Fig. 9f). Although Os concentrations are unavailable for HT lavas, LT lavas contain concentrations of a similar level to Ir in the same rocks (up to 1.2 ppb; Fig. 9a). Paranapanema lavas have the lowest Cu/Pd of the PELIP lavas (Fig. 10a), similar to the majority of NAIP lavas. Figure 10b The IPGE/PPGE enrichment split between LT and HT is such that LT lavas tent to have the lowest Pd/Ir ratios (Fig. 10b), in a similar range to most NAIP lavas from Hughes et al. (2015). Urubici and Pitanga magma-types evidently contain less PPGE compared to the LT samples in Figure 10b. Figure 10c and 10d compare PGE ratios to trace element signatures, to help characterise the chalcophile trends alongside magmatic differentiation trends from earlier figures.

4. Discussion

4.1. Magmatic trends

Our results show important geochemical trends across both the Peate et al. (1992) and Licht (2018) classification schemes that help contextualise precious metal trends, summarised and interpreted herein. Low MgO content (2-7 wt.%; Fig. 3a-h) and Ni concentrations (<125 ppm; Fig. 4a) across all Serra Geral lavas implies that they are not primary mantle melts and have undergone significant differentiation, likely via fractional crystallisation (Xiao et al., 2004). Mineral fractionation vectors in Figure 3a-h strongly suggest that olivine, clinopyroxene and plagioclase (plus minor amounts of spinel-group minerals) were progressively removed from the parent magmas leading to decreases in Fe_2O_3, CaO, MnO and Al_2O_3, and increases in incompatible Na_2O and K_2O with decreasing MgO content (Fodor, 1987; Peate et al., 1990). As observed in thin section, the dominant mineral in all mafic samples is orthopyroxene, with clinopyroxene, plagioclase and spinel-group minerals, and a notable absence

of olivine (typically 0-5% of assemblages), likely due to the earlier removal. Most major elements exhibit a single fractionation trend for each magma-type with a possible slight change in slope and groupings below ~4 wt.% MgO, indicating that the fractionating mineral(s) were reasonably consistent for mafic lavas. For TiO_2 and P_2O_5 (Fig. 3a and 3h), the fractionation trends indicate at least two liquid lines of descent, with Type 4 lavas (Urubici and Pitanga) exhibiting much more pronounced negative slopes with MgO compared with Type 1 lavas (Paranapanema, Esmeralda and Gramado), which are weakly negative. These branching fractionation trends indicate differing accessory/minor mineral constituents between magma-types and localities. We suggest that Type 4 lavas fractionated TiO_2 and P_2O_5-poor accessories such as chromite (which may also explain the more prominent Cr depletion with decreasing MgO in this group in Fig. 4d), while Type 1 lavas fractionated magnetite, titanomagnetite and/or apatite.

Olivine fractionation would efficiently remove compatible Ni ($D_{Ni}^{ol-melt}$ = 7.21) and Co ($D_{Co}^{ol-melt}$ = 2.28) (Spandler and O'Neill, 2010). Considering the Serra Geral mafic lavas are particularly olivine-deficient in thin section and reasonably evolved with respect to SiO_2 and MgO concentrations (45-60 wt.% and 2-7 wt.%, respectively; Fig. 2d and 3a-h), it is likely that a significant amount of compatible base metals have been removed from the parent magmas prior to eruption in all magma-types. In a similar manner, Cr is depleted in lavas throughout the region, which we attribute to the removal of both olivine and chrome spinel. Copper appears to be the only base metal/chalcophile retained in the lavas in any significant amount (Fig. 4b), and thus is neither strongly compatible nor incompatible in the fractionating silicate and oxide mineral phases. If sulphide fractionation drove chalcophile depletion, Cu would be uniformly removed from melts given its strong affinity for sulphide liquids in silicate melts ($D_{Cu}^{sulphide-melt}$ = 1,470; Mungall and Brenan, 2014). Since this is not the case, we propose that large degrees of olivine and chromite fractionation experienced by such MgO-depleted magmas would effectively remove Ni, Co and Cr while leaving Cu in melts.

Trace element concentrations and ratios provide evidence for markedly different geochemical processing between magma-types within the Serra Geral Group. Some Type 4 lavas feature as much as an order-of-magnitude enrichment in LREE compared to Type 1 lavas (particularly Southern), indicating differing degrees of partial melting or assimilation of continental crust (Fig. 5a-f). Combined with the trends of HT lavas towards OIB signatures in Figure 6b and high-Ti melts akin to Karoo CFBs in Figure 6c, we suggest Type 4 represents more strongly plume-related magmas in agreement with Rämö et al. (2016), who attribute HT lava $^{87}Sr/^{86}Sr$ and εNd signatures to an enriched mantle (EM1) component. Given that the HT/Type 4 lavas align with the plume focus ca. 135 Ma (Beccaluva et al., 2020), their signatures in our study signify the strongest asthenospheric signal.

More pronounced negative Eu anomalies in the LT group than HT lavas (Fig. 5) indicate that a larger amount of plagioclase fractionated from the parent magma, signalling a higher degree of crystal fractionation (FC) in this group compared to HT. The LT lavas, particularly Gramado, exhibit decreasing Nb/La with increasing SiO_2 (Fig. 6a), indicating the role of assimilation and fractional crystallisation (AFC) in the parent magmas. The depletion in trace element signatures and strongly negative Ta-Nb anomalies (Figs. 7d-e) indicate that contamination by continental crust material during magma ascent may have been important in their geochemical development, as widely documented by isotopic studies of the LT group (e.g. Peate et al., 1992; Rocha-Júnior et al., 2013; Natali et al., 2017; Marques et al., 2018). The Ta-Nb anomalies in HT lavas (Fig. 7a-c) are significantly less pronounced, indicating a lower degree of crustal contamination in these magmas. Chapecó and Palmas typically trend with HT and LT, respectively, in Figures 5f, 6a-d and 7f, suggesting they share a common source and perhaps evolved towards silicic compositions from their associated mafic magma-types.

Trace element observations provide an initial indication, prior to quantitative modelling, of melting conditions for the Serra Geral magmas. The steeply negative medium to HREE-LREE trends for Type 4 multi-element patterns in Figures 5a-b, along with Type 4 samples trending towards high $(Sm/Yb)_n$ values in Figure 6d suggest low degrees of partial melting and HREE retention in residual garnet. This

could imply high pressure melting conditions commonly associated with plume melts beneath thick continental cratons, where the majority of the melting occurs in the garnet-bearing asthenosphere (e.g. Arndt et al., 1998; Jourdan et al., 2007). In comparison, Type 1 lavas are strongly associated with trace element trends produced by the melting of spinel peridotite (Fig. 6d) (e.g. White and McKenzie, 1995), which corresponds with their shallow medium to HREE slopes in Figures 5c-e. Paranapanema lavas trend with Type 1 (Southern) towards spinel peridotite melts (Fig. 6d), exhibit medium to heavy REE slopes between those Type 1 (Southern) and Type 4, but are grouped with Type 4 OIB sources in other discriminant diagrams (e.g. Fig. 6c) and as such must be regarded separately in terms of source interpretation, as in Licht (2018).

The spinel to garnet transition occurs where pressures and temperatures exceed 3 GPa and 1,570°C (Milholland and Presnall, 1998; Walter et al., 2002). This translates to depths of 50-70 km in asthenospheric regions and 120-180 km in colder sub-cratonic settings (Kent and Fitton, 2000; Ziberna et al., 2013). In Cr-rich mantle sources or depleted rocks such as harzburgite, the transition can occur at significantly higher pressures (up to 10 GPa) and typically increases the depths at which spinel and garnet are both stable simultaneously (Klemme, 2004; Ziberna et al., 2013). The different spinel/garnet melting trends exhibited by the Serra Geral lavas reflect either 1) different degrees of melting of a garnet-bearing mantle source (with garnet exhaustion in the most extreme cases) or 2) separate melting sources and depths (between 50 and 100 km; Gibson et al., 2006) as a function of the rapidly evolving geodynamic setting. Both scenarios would require a change in melting depth between magma-types, to facilitate differential degrees of partial melting (Beccaluva et al., 2020), and polybaric melting processes are favoured by Rämö et al. (2016) in their assessment of Pitanga and Paranapanema geochemical differences. We model the trace element geochemistry of Serra Geral lavas, including chalcophile elements, in Section 4.2.3, after firstly interpreting PGE enrichments in relation to partial melting information.

4.2. PGE enrichment

Trends in PGE enrichment fall consistently into the three major mafic subdivisions established by Licht (2018) in Figures 8 and 9 – Pitanga and Urubici in Type 4, Paranapanema in Type 1 (Central-Northern), and Gramado and Esmeralda in Type 1 (Southern). As such, it is most appropriate to primarily use these newer classifications in lieu of the classic groups when discussing metallogenesis going forward.

Type 1 (Southern) lavas are more enriched in IPGE than all other lavas (Fig. 8a-f). This is especially true for Ru concentrations, which are an order of magnitude higher than typical intracontinental lavas (Barnes et al., 2015). Furthermore, Rh, the transitional PGE that shares properties with both IPGE and PPGE (Barnes et al., 1985; Holwell and McDonald, 2010 and references therein), is also enriched in Type 1 (Southern) lavas, forming a 'humped' shape on their plots in Figure 8d-e. Contrasting this trend to the notable Pd and Au enrichment (and steep slope in the multi-element diagram) in the Type 1 (Central-Northern) lavas (Fig. 8c) and general depletion in PGE in Type 4 lavas (Fig. 8a-b), it is clear that PGE signature are heterogeneous in the region. The discrepancy with depleted Ni and Co, and relatively enriched Cu in Figure 4a and 4b supports preferential fractionation of Ni and Co via olivine, in the absence of significant Cu depletion via sulphide removal. As noted in Section 4.1, we suggest that sulphide fractionation did not control base metal and PGE concentrations in the PELIP magmas. Thus, we must identify different geochemical sources outside sulphide depletion to explain the separate Ir-Ru-Rh and Pd-Au-Cu enrichment associations in Type 1 lava varieties that make sense when integrated with their major and trace element interpretations.

4.2.1.Palladium in Type 1 (Central-Northern) lavas

The Pd-Au-Cu enrichment in Type 1 (Central-Northern) samples is clearly illustrated by their steep multi-element slope in Figure 8c and high Pd/Ir ratios in Figure 10b, which place the lavas as 1-2 orders of magnitude more Pd-rich than all other lavas in this study. These lavas often contain up to 30 ppm more Pd than any other group (Fig. 9f), particularly Type 4, and contain slightly higher mean Cu and Au concentrations than others (Figs. 4b and 10f). Given that Pd, Cu and Au are all mobile incompatible chalcophiles commonly associated with each other in fluid-rich environments (e.g. Holwell et al., 2019;

Choi et al., 2020 and references therein), we propose that Pd, Cu and Au-bearing material is being preferentially incorporated into Type 1 (Central-Northern) melts. This supports Type 1 (Central-Northern) as a separate compositional group by Licht (2018) despite earlier classification alongside Urubici and Pitanga by Peate et al. (1992); the fundamental geochemical controls on Si, Ti, Zr and P in Serra Geral magmas established from this study evidently have an impact on PGE concentrations. Enrichment in Pd-Cu-Au is unique to Type 1 (Central-Northern) lavas in the PELIP and thus a different partial melting model is required to generate the compositional variances from other samples. If, as suggested by Rocha-Júnior et al. (2013), the significant stratigraphic and spatial distance between the eruption of individual magma-types represents physically distinct sources in the mantle, we would expect each of the parental magmas to feature their own set of geodynamic controls on geochemistry.

The three metals enriched in Type 1 (Central-Northern) lavas - Pd, Au and Cu - are notable for being more incompatible in silicate melting environments than the other five PGE and base metals (e.g. Mitchell and Keays, 1981; Borisov et al., 1994; Holzheid et al., 2000; Righter et al., 2008; Tassara et al., 2017). Furthermore, Pd does not form micronuggets like the other PGE, tending to exist in base metal sulphides alongside Cu and Au (Holzheid et al., 2000). Metasomatic activity can easily redistribute such metals via fluids and melts at the upper mantle and base of the lithosphere in sub-cratonic settings over long periods of time (e.g. Zhang et al., 2008; Maier and Groves, 2011). Given that the Paraná Basin exists on Proterozoic Gondwanan basement, the SCLM beneath modern day Brazil will have been subjected to numerous fertilisation events (Rocha-Júnior et al., 2013) via subduction around the cratonic margin (Tassara et al., 2017). Subducting oceanic crust can release mobile elements in dehydrating fluids or small-degree melts as the plate descends, and these become concentrated in a mantle wedge and SCLM (e.g. Woodland et al., 2002; Griffin et al., 2013; Tassara et al., 2017; Rielli et al., 2018; Wade et al., 2019), similar to the origins of Cu-porphyry environments. Metasomatic sulphide minerals, and by extension chalcophile elements, can then be scavenged by melts generated in an intracontinental setting (Powell and O'Reilly, 2007). Generally, Pd will follow Cu during partial melting of the mantle and can be found in similar sulphide phases at upper mantle P/T conditions (e.g.

Barnes et al., 1997; Mungall et al., 2005; Lorand et al., 2013 and references therein). If Cu- and Pd-bearing sulphides are melted and incorporated into magmas interacting with the SCLM, the two metals can share a coupled enrichment in resulting volcanic and intrusive products (e.g. Bockrath et al., 2004; Alard et al., 2011; Delpech et al., 2012; Lorand et al., 2013; Lorand and Luguet, 2016; McDonald et al., 2017; Tassara et al. 2017).

An alternative theory is that whilst the SCLM still received enrichment via metasomatic processes, subduction did not supply the metals. In Figure 11a-b, relative PGE concentrations are compared to classic sub-lithospheric rocks from the literature, pyroxenite xenoliths from Cameroon (Abeng et al., 2012). Here, Type 1 (Central-Northern) samples plot far from classic intraplate xenoliths and instead are much more alike the pyroxenites. Thus, the enrichment of PPGE in the parent magma could have resulted from pyroxenite (i.e., recycled oceanic crust components) in the melt column and/or SCLM. Given the long history of the Gondwanan SCLM likely including many metasomatic and partial melting events, and the tendency of mantle plumes to sample both pyroxenite and peridotite from the deep mantle, this is plausible, yet would require Os-isotope data to accurately confirm. Regardless of mechanism (subduction or mantle component-driven), the Type 1 (Central-Northern) parent magmas require enrichment in PPGE, Cu and Au prior to ascent via a metasomatic event to produce such PGE signatures.

In a study comparing intracontinental melts from depleted asthenospheric and metasomatised SCLM sources in the North China Craton, Wang et al. (2020) determined that the latter were 3-4 times more enriched in precious and base metals, likely via efficient extraction of SCLM sulphides during melting. Furthermore, spinel lherzolite xenoliths in intracontinental lavas from Ethiopia (Lorand et al., 2003), showing evidence of metasomatic deformation and melt percolation, acquired a characteristic enrichment in S-Cu-Pd-Au. Given the unique geochemical characteristics of Type 1 (Central-Northern) lavas for the PELIP, our metallogenic model must provide a mechanism for differentiating the magma-type from the others, particularly the Type 1 (Southern) group given that they melt at a similar depth

according to garnet-spinel information in Figure 6d. We propose that given the documented metasomatic association of Pd and Cu (e.g. Hughes et al., 2014; Tassara et al., 2017; Holwell et al., 2019; Choi et al., 2020) and potentially Au (although this is less constrained; Maier et al., 2012), and the consistently higher concentrations in shallower-derived continental melts from the PELIP (e.g. potentially involving more SCLM than asthenosphere), the Type 1 (Central-Northern) lavas obtained elevated concentrations of Pd, Cu and Au by the passive melting of metasomatised SCLM by the Tristan plume. Indeed, studies of Brazilian mantle xenoliths indicate a protracted metasomatic history beneath the craton (e.g. Rivalenti et al., 2000; Carlson et al., 2007), supporting this hypothesis.

4.2.2.Ruthenium and rhodium in Type 1 (Southern) lavas

The plateau between Ru, Rh and Pt in Type 1 (Southern) samples (Fig. 8d-e) likely reflects the source minerals included in parental melts. This likely indicates that a Ru-Rh-bearing mineral(s) is being incorporated into Type 1 (Southern) magmas from a mantle source in a separate system from other magmas. The melting depth and source for Type 1 magmas are different to Type 4 (Rämö et al., 2016; Licht, 2018) (Fig. 6d), implying distinct melting processes in the northern and southern basalts (Beccaluva et al., 2020) that could explain the groups' differing metallogenic characters. Overall, the PGE behave in a similar manner chemically – in the presence of a sulphide melt portion, all six will be overwhelmingly concentrated within it rather than the silicate melt. However, the individual partition coefficients of the PGE between silicate minerals and melt vary significantly when not in the presence of sulphides (e.g. Peach et al., 1990; Peach et al., 1994; Righter et al., 2004; Park et al., 2017 and references therein), and the melting of a sulphide-deficient mantle will facilitate the heterogeneous incorporation of PGE into melts. It follows that the enrichment and depletion of PGE in Serra Geral lavas must be controlled by silicate or oxide differentiation processes in the magma. If the melts were depleted in sulphide, the majority of their PGE basket would also be removed and they would have higher Cu/Pd than what is displayed in Figure 10a, more common in NAIP magmas. To add Ru and Rh

to Type 1 (Southern) in the quantities observed in Figures 8d-e and 9c-d would require melting of a source rich in these PGE alone, or at least in higher proportions than the other PGE.

Type 1 (Southern) and (Central-Northern) lavas follow a liquid line of descent commonly associated with the melting of spinel peridotites at shallower depths and lower pressures than Type 4 magmas (Figs. 6d). Experimental studies found Ru and Rh to be compatible in spinel-group minerals (Capobianco and Drake, 1990; Barnes and Picard, 1993; Pitcher et al., 2009), with spinel-silicate melt partition coefficients of 400-900 (Righter et al., 2004). This synchronises well with our trace element ratios (Fig. 6) – by melting a source with normative spinel-group mineral content, the generated magma would contain relatively high concentrations of the two PGE. In the mantle, Os, Ir, Ru and Rh are also highly compatible in sulphides, platinum-group minerals (PGM) and alloys, different mineral phases from the base metal sulphides, tellurides and arsenides that Pt and Pd are commonly found in (e.g. Mitchell and Keays, 1981; Alard et al., 2000; Helmy and Bragagni, 2017; Helmy and Fonseca, 2017). As such, the variety of sulphide compositions in the mantle source can be a crucial factor in fractionating the PGE from each other and isolating an IPGE and Rh rich mineral phase (i.e. Ni-sulphides, alloys or even spinel) for preferential melt incorporation (e.g. Keays et al., 1982; Barnes and Picard, 1993; Rehkämper et al., 1997; Maier et al., 2003). A combination of spinel-group minerals and IPGE-sulphides at source may provide the necessary PGE signatures to Type 1 (Southern) melts. However, Type 1 (Central-Northern) sample trace element signatures also indicate spinel peridotite as a melting source in Figure 6d, cluster with Type 1 (Southern) in Figure 6b, and sit distinct from the other magma-types in the Licht (2018) study. Type 1 (Central-Northern) lavas do not have the characteristic Ru-Rh enrichment in Figures 8c and 9c-d. This suggests that although all Type 1 lavas likely formed by the partial melting of spinel peridotite mantle, the melting processes for the Southern and Central-Northern varieties must have been different to incorporate a different suite of PGE, or the mantle sources being melted exhibited different metasomatic characters.

4.2.3. Modelling melt compositions

Based on the interpretations of all Type 1 lava PGE signatures, we forward-modelled melt compositions appropriate for melting of primarily spinel peridotite in a sub-lithospheric setting, using mass balance calculations from Shaw (1970) and experimental melting mode values from Johnson (1998) (Fig. 12a-b). Mineral-melt partition coefficient sources are given in Figure 12 and Table 2. Starting with bulk concentrations of Co, Ni, Cu, PGE and Au from i) metasomatised arc, ii) normal arc, iii) cratonic, and iv) off-craton peridotite xenoliths collated by Barnes et al. (2015), and the mineral mode (X) and melt mode (p) values displayed in Table 2, we successfully generated chondrite-normalised multi-element PGE plots representative of the Serra Geral Type 1 magmas (summarised in Figure 12; see Supplementary E for further details). Metasomatised and normal arc xenoliths represent re-enriched and depleted upper mantle sources in our Type 1 (Central-Northern) models, respectively. On-craton xenoliths are generally from kimberlites within the thickest area of a craton block whilst off-craton are from kimberlites in thinner mobile belts surrounding cratons (e.g. Wildman et al., 2017); these represent a progressively thinning intracontinental setting in our Type 1 (Southern) models.

An important caveat for our models is that strongly chalcophile elements (such as the PGE) will preferentially stay in sulphide minerals until the phase is melted entirely, and as such, sulphide melting strongly controls the concentration of PGE in the resulting magmas. In order to attain PGE concentrations contained in any of our samples (between 0.0001 and 0.1 x chondritic; Fig. 8a-f), the sulphide phase, if present in the source (~1 wt.% in our model), must be exhausted. Similarly, for IPGE and Rh compatible in spinel, this mineral phase must be entirely melted to release the metals into magmas. Given the spinel-melt partition coefficients for IPGE are often 3-4 orders of magnitude smaller than those for sulphides (Table 2), the effect on resulting concentrations pre-exhaustion is much less pronounced. Further, it must be noted that chalcophile sulphide-melt partition coefficients can be highly variable from experiment to experiment, so we have maintained those found by Mungall and Brenan (2014) for consistency whilst acknowledging the challenges of modelling sulphide melts.

PGE, Cu, Co and Ni concentrations progressive melting are given in bivariate plots in Supplementary E for each scenario, in support of Figure 12.

To generate Type 1 (Central-Northern) magmas, our models (Fig. 12a) show that elevated bulk Cu, Pt, Pd and Au concentrations in the source strongly influence the resulting melt enrichment. Metasomatised continental arc xenoliths (as in Wilson et al., 1996) typically feature such enrichment of Cu, Pt, Pd and Au. Beneath ancient cratons, the SCLM can be pre-conditioned by repeated subduction events throughout history (e.g. Mitchell and Keays, 1981; Powell and O'Reilly, 2007; Zhang et al., 2008; Hughes et al., 2014; Hughes et al., 2015; Holwell et al., 2019). The model predicts that at melting degrees of around 20 %, metasomatic sulphides in an arc-like mantle will be exhausted at the conditions from Table 2, releasing chalcophile elements into the melt ('metasomatised arc' in Fig. 12a). Identical melting conditions with a less Pt, Pd, Au and Cu-enriched source would produce chondrite-normalised plots with shallower gradients ('normal arc' in Fig. 12a, also from Wilson et al., 1996), indicating that bulk source composition is the key factor in melt enrichment. Further, a mantle source without sulphide in the mineral mode cannot sufficiently produce melts with elevated Pt, Pd or Au concentrations, as the elements in question do not partition strongly into the remaining silicate or oxide mineral phases. It should be noted that PGM and alloys are also known to host small amounts of the SCLM's PGE budget (e.g. Hughes et al., 2015; González-Jiménez et al., 2020), but our model does not account for these phases. If Brazilian SCLM *does* host Pd-bearing PGM this would only work to boost our model further and reinforce the idea of metasomatically-enriched Pd-Au-Cu SCLM components.

Cratonic (Maier et al., 2012) and off-cratonic (Schmidt et al., 2003) peridotite xenoliths have a more even distribution in PGE concentrations, but in most cases are enriched in Ir, Ru and Rh, and depleted in Pt, Pd and Au with respect to arc sources (Table 2). Our models predict that once sulphides are exhausted, the resulting on/off craton melts produce nearly flat chondrite-normalised PGE-enrichment patterns (Fig. 12b), but not the Ru-Rh 'hump' from Fig. 8d-e. However, given that evidence

shows that Type 1 lavas were derived from melts nearer the locus of lithospheric rifting (Beccaluva et al., 2020), we assume a higher-degree (i.e 25 %) melt fraction in the off-craton setting (i.e. thinner lithosphere, shallower/higher degree partial melts) as a best fit the PGE patterns in our Gramado and Esmeralda samples. This allows more spinel to be melted which increases Ir, Ru and Rh concentrations to match Type 1 (Southern) patterns (Fig. 8d-e). In the absence of sulphide, our model can produce similar PGE enrichment curves, implying that these lavas, unlike Type 1 (Central-Northern), do not rely on metasomatic sulphides in the melting system. Elevated source bulk concentrations in the relevant metals are the key driver in resulting melt composition in all models, provided the host phase can be sufficiently melted.

Our modelling demonstrates that Type 1 (Central-Northern) magma compositions are best explained by a mantle source region with metasomatic sulphides which become exhausted during partial melting, while Type 1 (Southern) magmas can be generated by higher degrees of partial melting to exhaust *both* sulphides and spinel-group minerals (if sulphides were present at all). Locally heterogeneous SCLM beneath Brazil (Fodor et al., 2002; Carlson et al., 2007), as exists in other CFB provinces worldwide (Karoo in Jourdan et al., 2007; Emeishan in Song et al., 2008; the North Atlantic in Hughes et al., 2015; and South Australia in Wade et al., 2019), can generate diverse PGE signatures in melting signatures.

4.3. Melt components and the role of the SCLM in CFB metallogenesis

A unifying metallogenic model for Serra Geral must incorporate aspects of geodynamic, mineralogical and melting models to explain major and trace element signatures in the region. The variable enrichment and depletion of PGE and Au in Paraná CFB magma-types immediately characterises Type 4 (the highest-Ti magma-type of the HT group) as relatively deficient in all seven precious metals. In contrast, the Type 1 mafic magma-types contain the modelled enrichments in two different sets of PGE/chalcophiles – Pd, Au and Cu in Type 1 (Central-Northern), and Ru and Rh in Type 1 (Southern). The concentrations can be explained by variable element compatibility and mineral assemblages

expected in the melting region (Figs. 12a-b), which in turn implies changing conditions beneath the Tristan plume. Between the generation of Type 4 and Type 1, the mantle source has changed to distinctly spinel lherzolite (Fig. 6d) (in agreement with Rämö et al., 2016). This indicates a progressive shift to shallower melting depths, which may have allowed higher degrees of partial melting (i.e. 20-25 %, as modelled in Fig. 12a-b), permitting access to different zones and/or greater amounts of the SCLM as a melting source. We propose a multi-component metallogenic model (Fig. 13) to describe the incorporation of variable PGE assemblages throughout the geochemical magma-types in the Paraná CFB, in line with the region's geodynamic development in the Cretaceous (135-128 Ma; Fig. 1a-b) and modelling from Figure 12.

Firstly, we must establish the evolving geodynamic setting in Cretaceous Brazil as the mechanism behind the differing PGE enrichment. Prior to extension, a thick continental lithospheric 'lid' suppressed the degree of melting beneath the Gondwanan continent and confined CFB melt generation to deeper in the upper mantle (i.e. at the plume head), firmly within the upper mantle garnet lherzolite stability field (as in Arndt et al., 1993; White and McKenzie, 1995; Turner et al., 1996; Kerr, 1997). Following lithospheric thinning as a consequence of thermal weakening by the underlying mantle plume and the onset of continental rifting from the south-east ca. 134 Ma, the underlying mantle decompressed and enabled partial melting at shallower depths i.e. within the spinel lherzolite stability field (e.g. Ellam, 1992; Stein and Stein, 1992). This thinning would be most prevalent in south-eastern Paraná, near the future Atlantic coast, forming geographically-bound differences in lithospheric thickness and melting depth (Turner et al., 1996), decreasing from the north-west (HT lavas) to the south-east (LT lavas) (Beccaluva et al., 2020). This echoes the geodynamic setting of the Palaeogene proto-Icelandic rift-plume system in the North Atlantic – magmas from under the intact Greenlandic lithosphere and magmas at/near the developing Atlantic rift zone record different depths of melting and markedly different melt geochemistry as a result (e.g. Saunders et al., 1997; Kent and Fitton, 2000; Hughes et al., 2015; Lindsay et al., 2020). The transition from thick North Atlantic Craton to rifted lithosphere resulted in high- then low-Ti continental magma generation (Momme et al.,

2006), reflected in their apparent depth and degree of melting, and garnet/spinel source signatures. In the case of Paraná, we propose that partial melts that are generated at the garnet-spinel transition as a function of lithosphere extension can directly control the variable metal baskets in the Serra Geral magma-types as modelled (in line with Kerr, 1995; Klemme and O'Neill, 2000; Gibson et al., 2006). Although Serra Geral lavas generally follow the classic stratigraphy of Gramado to Esmeralda and Palmas (with minor Urubici intercalated) in the south and Pitanga to Paranapanema and Chapecó in the north (Fig. 1c), it must be reiterated that the lavas are synchronous across the Paraná Basin. Evidence for synchronicity includes mixing between Esmeralda and Pitanga (De Min et al., 2017), Urubici occurrence between successive Gramado layers (Turner et al., 1996) and Paranapanema underlying the 'older' Gramado in places (Turner et al., 1999). The ongoing development and diversification of the magmas does not necessarily equate to their complex temporal and spatial surface distribution sequence.

The smaller degree of crustal contamination and more enriched mantle melt signatures place Type 4 lavas as close to a plume component as possible in the region, such that Urubici and Pitanga lavas are enriched in LREE and incompatible elements (Figs. 5a-b and 7a-b). Through time, as the lithosphere thinned, the melting region shifted to shallower depths in response to the lid effect, producing Type 1 (Central-Northern) magmas from a HT source (albeit with a drop in bulk TiO_2 concentration), evidenced by the transition from garnet to garnet-spinel to spinel lherzolite (Fig. 6d) (Rämö et al., 2016). These melts successfully incorporated metasomatised (i.e. Pt, Pd, Au and Cu bearing) SCLM sulphides given the presumed increased degree of melting possible at reduced depths, modelled in Figure 12a. Silicic Chapecó magmas that were formed by small degree partial melt extraction from the HT magmas would not inherit the Pd, Au or Cu concentrations contained within Type 1 (Central-Northern) because their subsequent upper crustal development would have fractionated such elements into early crystals and removed them from the felsic system. It is unclear whether the differences in melting depth were a) progressive from a single evolving and shallowing melting site or

b) spatially distinct despite the general 'northern' HT source. Given the synchronous nature of Serra Geral lavas, we opt for the latter view.

Further to the east, Type 1 (Southern) magmas were sourced from beneath thinner lithosphere still, near the Atlantic rift and further from the plume focus – this produced higher degree partial melts within the spinel lherzolite mantle (Fig. 6d) with much more dilute TiO_2 concentrations (Fig. 3a). These higher-degree melts were able to exhaust sulphide and spinel, to produce the IPGE and Rh dominant signatures in Figures 8d-e and 12b. Beccaluva et al. (2020) suggest that where HT magmas were less viscous and were able to rise to the surface with minor assimilation of crustal material, LT magmas stalled in subsurface chambers prior to eruption. All LT Type 1 (Southern) lavas consequently exhibit geochemical evidence for contamination, such as high $^{87}Sr/^{86}Sr$, low εNd and crustal U-Th-Pb isotopic signatures (Peate, 1997). The transition from Gramado to Esmeralda within Type 1 (Southern) did not visibly affect PGE concentrations (Figs. 9a-f). Palmas lavas formed from protracted upper crustal development of LT lavas, in this case with more extensive AFC than the mafic melts (Garland et al., 1995; Milner et al., 1995), which may explain the loss of PGE from parental Type 1 magmas.

Overall, the shifting melting depth imposed by the Tristan plume in response to the breakup of Gondwana drives regional metallogenesis. It is highly likely that the SCLM beneath Brazil is heterogeneous in terms of precious metal content hosted in metasomatic sulphide phases in the mantle. Whilst Type 4 magmas did not receive 'spiked' PGE signatures from increased degrees of melting, the shallower-sourced Type 1 melts exhausted sulphides and, for the Southern magmas, spinel-group minerals to attain elevated precious metal contents. The scale of the PELIP, localised nature of metasomatism, and synchronicity of geochemically diverse regional lavas reinforces the idea that a variety of concurrent magmatic systems worked in unison to produce the complex stratigraphy of Serra Geral.

5. Conclusions

The bulk major and trace element, PGE and Au data and quantitative modelling presented in this chapter support a progressively thinning lithosphere in response to thermal uplift from the upwelling Tristan plume and congruent crustal extension. This in turn directly affects the depth and source of Paraná intracontinental partial melts and their resulting metal baskets.

1. Serra Geral Type 4 lavas (i.e., Urubici and Pitanga) do not contain any significant enrichment in precious metals, primarily due to their origin as deeper asthenospheric melts with plume-derived trace element enrichments but no obvious precious metal contribution from the SCLM.
2. Serra Geral Type 1 (Central-Northern) lavas (i.e., Paranapanema) contain elevated Pd concentrations, coupled with higher mean Au and Cu than the other magma-types, which we attribute to a shallower melting environment, but still primarily within the asthenosphere, promoting the incorporation of metasomatically-enriched Proterozoic SCLM.
3. Serra Geral Type 1 (Southern) lavas (i.e., Gramado and Esmeralda) display unique Ru-Rh enrichment that can be linked to shallow SCLM melting at the developing rift zone, and spinel and/or sulphide incorporation from the melting source.
4. The heterogeneous PGE enrichment of cratonic SCLM by metasomatism in intracontinental settings, as exhibited beneath the North Atlantic Igneous Province, the North China Craton and Ethiopia, promotes variable metallogenic characters throughout CFB provinces. This highlights the crucial role of plume-SCLM interaction as a potential precursor to the generation of PGE ore deposits in the upper crust from intracontinental magmas.

Acknowledgements

The authors would like to thank Chris Hawkesworth for his expert insights into all things plume-related and for his continued support throughout this project. We would also like to thank Gavyn Rollinson, Malcolm Spence, Sharon Uren, Steve Pendray, and Katie McFall for their invaluable assistance in lab work, and Matthew Head for helping set up initial coding in Mat Lab. Finally, we would like to thank all at Universidade Federal do Paraná and Serviço Geológico do Brasil in Curitiba for being so

welcoming, and for making our field excursions so interesting and enjoyable with their local knowledge. Wolfgang Maier, Peter Lightfoot and an anonymous third reviewer are thanked for their immensely useful and thorough reviews that significantly enhanced the quality of this paper. JJL is sponsored by the University of Exeter's Vice-Chancellor Scholarship for Post-Graduate Research.

References

Abeng S. A. E., Ndjigui P-D., Beyanu A. A., Teutsong T. and Bilong P. (2012) Geochemistry of pyroxenites, amphibolites and their weathered products in the Nyong unit, SW Cameroon (NW border of Congo craton): Implications for Au-PGE exploration. *J. of Geochem. Explor*. **114**, 1-19.

Alard O., Griffin W. L., Lorand J. P., Jackson S. E. and O'Reilly S. Y. (2000) Non-chondritic distribution of the highly siderophile elements in mantle sulphides. *Nature* **407**, 891–894.

Alard O., Lorand J. P., Reisberg L., Bodinier J. L., Dautria J. M. and O'reilly S. Y. (2011) Volatile-rich metasomatism in montferrier xenoliths (Southern France): Implications for the abundances of chalcophile and highly siderophile elements in the subcontinental mantle. *J. Petrol.* **52**, 2009–2045.

Andersen J. C. Ø., Power M. R. and Momme P. (2002) Platinum-Group Elements in the Palaeogene North Atlantic Igneous Province. The geology, geochemistry, mineralogy, and mineral beneficiation of platinum-group elements. *L. J. Cabri. Montréal, Québec, Can. Inst. Mining, Metall. Pet.* **CIM Spec.**, 637–667.

Arndt N., Chauvel C., Czamanske G. and Fedorenko V. (1998) Two mantle sources, two plumbing systems: Tholeiitic and alkaline magmatism of the Maymecha River basin, Siberian flood volcanic province. *Contrib. to Mineral. Petrol.* **133**, 297–313.

Arndt N. T., Czamanske G. K., Wooden J. L. and Fedorenko V. A. (1993) Mantle and crustal contributions to continental flood volcanism. *Tectonophysics* **223**, 39–52.

Barnes S. J., Makovicky E., Makovicky J., Rose-Hansen J. and Karup-Moller S. (1997) Partition coefficients for Ni, Cu, Pd, Pt, Rh, and Ir between monosulfide solid solution and sulfide liquid and the formation of compositionally zoned Ni – Cu sulfide bodies by fractional crystallization of sulfide liquid. *Can. J. Earth Sci.* **34**, 366–374.

Barnes S. J., Mungall J. E. and Maier W. D. (2015) Platinum group elements in mantle melts and mantle samples. *Lithos* **232**, 395–417. Available at: http://dx.doi.org/10.1016/j.lithos.2015.07.007.

Barnes S. J., Naldrett A. J. and Gorton M. P. (1985) The origin of the fractionation of platinum-group elements in terrestrial magmas. *Chem. Geol*. **53**, 303–323.

Barnes S. J. and Picard C. P. (1993) The behaviour of platinum-group elements during partial melting, crystal fractionation, and sulphide segregation: An example from the Cape Smith Fold Belt, northern Quebec. *Geochim. Cosmochim. Acta* **57**, 79–87.

Beattie P., Ford C. and Russell D. (1991) Partition coefficients for olivine-melt and orthopyroxene-melt systems. *Contrib. to Mineral. Petrol.* **109**, 212–224.

Beccaluva L., Bianchini G., Natali C. and Siena F. (2020) Plume-related Paranà-Etendeka igneous province: An evolution from plateau to continental rifting and breakup. *Lithos* **362–363**, 105484. Available at: https://doi.org/10.1016/j.lithos.2020.105484.

Bellieni G., Comin-Chiaramonti P., Marques L. ., Melfi A. J., Piccirillo E. . and Nardy A. J. (1984) High- and low-TiO2 flood basalts from the Paraná plateau (Brasil): Petrology and geochemical aspects bearing on thier mantle origin. *Neues Jahrb. für Mineral.* **150**, 273–306.

Besser M. L., Maria E., Vasconcellos G., José A. and Nardy R. (2018) Morphology and stratigraphy of Serra Geral silicic lava flows in the northern segment of the Torres Trough , Paraná Igneous Province. *Brazilian J. Geol.* **48**, 201–219.

Bierlein F. P., Groves D. I. and Cawood P. A. (2009) Metallogeny of accretionary orogens - The connection between lithospheric processes and metal endowment. *Ore Geol. Rev.* **36**, 282–292. Available at: http://dx.doi.org/10.1016/j.oregeorev.2009.04.002.

Bockrath C., Ballhaus C. and Holzheid A. (2004) Fractionation of the platinum-group elements during mantle melting. *Science (80-.).* **305**, 1951–1953.

Borisov A., Palme H. and Spettel B. (1994) Solubility of palladium in silicate melts: Implications for core formation in the Earth. *Geochim. Cosmochim. Acta* **58**, 705–716.

Brenan J. M., McDonough W. F. and Dalpé C. (2003) Experimental constraints on the partitioning of rhenium and some platinum-group elements between olivine and silicate melt. *Earth Planet. Sci. Lett.* **212**, 135–150.

Burke K., Steinberger B., Torsvik T. H. and Smethurst M. A. (2008) Plume Generation Zones at the margins of Large Low Shear Velocity Provinces on the core-mantle boundary. *Earth Planet. Sci. Lett.* **265**, 49–60.

Camboa L. A. P. and Rabinowitz P. D. (1984) The evolution of the Rio Grande Rise in the southwest Atlantic Ocean. *Mar. Geol.* **58**, 35–58.

Capobianco C. J. and Drake M. J. (1990) Partitioning of ruthenium, rhodium, and palladium between spinel and silicate melt and implications for platinum group element fractionation trends. *Geochim. Cosmochim. Acta* **54**, 869–874.

Carlson R. W., Araujo A. L. N., Junqueira-Brod T. C., Gaspar J. C., Brod J. A., Petrinovic I. A., Hollanda M. H. B. M., Pimentel M. M. and Sichel S. (2007) Chemical and isotopic relationships between peridotite xenoliths and mafic-ultrapotassic rocks from Southern Brazil. *Chem. Geol.* **242**, 415–434.

Choi E., Fiorentini M. L., Hughes H. S. R. and Giuliani A. (2020) Platinum-group element and Au geochemistry of Late Archean to Proterozoic calc-alkaline and alkaline magmas in the Yilgarn Craton, Western Australia. *Lithos* **374–375**, 105716. Available at: https://doi.org/10.1016/j.lithos.2020.105716.

Cordani U. G. and Vandoros P. (1967) Basaltic Rocks of the Paraná Basin. In *Problems in Brazilian Gondwana Geology* (eds. J. J. Bigarella, R. D. Becker, and J. D. Pinto). pp. 207–231.

Courtillot V., Davaille A., Besse J. and Stock J. (2003) Three distinct types of hotspots in the Earth's mantle. *Earth Planet. Sci. Lett.* **205**, 295–308. Available at: /Users/cbeghein/Documents/PDFs/2003_Courtillot_Earth_and_Planetary_Science_Le.pdf%5Cn http://dx.doi.org/10.1016/S0012-821X(02)01048-8.

Delpech G., Lorand J. P., Grégoire M., Cottin J. Y. and O'Reilly S. Y. (2012) In-situ geochemistry of sulfides in highly metasomatized mantle xenoliths from Kerguelen, southern Indian Ocean. *Lithos* **154**, 296–314. Available at: http://dx.doi.org/10.1016/j.lithos.2012.07.018.

Deschamps F., Kaminski E. and Tackley P. J. (2011) A deep mantle origin for the primitive signature of ocean island basalt. *Nat. Geosci.* **4**, 879–882. Available at: http://dx.doi.org/10.1038/ngeo1295.

Downes H. (2001) Formation and modification of the shallow sub-continental lithospheric mantle: A review of geochemical evidence from ultramatic xenolith suites and tectonically emplaced ultramafic massifs of Western and Central Europe. *J. Petrol.* **42**, 233–250.

Eldholm O. and Grue K. (1994) North Atlantic volcanic margins : Dimensions and production rates a volume of flood basalts a mean eruption rate of the basalts were emplaced within volume in a mean crustal accretion rate. *J. Geophys. Res.* **99**, 2955–2968.

Ellam R. M. (1992) Lithospheric thickness as a control on basalt geochemistry. *Geology* **20**, 153–156.

Evans N.J., Davis J. J., Byrne J. P. and French D. (2013) Contamination-free preparation of geological samples for ultra-trace gold and platinum-group element analysis. *Journal of Geochemical Exploration.* **80** (1), 19-24.

Fodor R. V. (1987) Low- and high-TiO2 flood basalts of southern Brazil: origin from picritic parentage and a common mantle source. *Earth Planet. Sci. Lett.* **84**, 423–430. Available at: https://linkinghub.elsevier.com/retrieve/pii/0012821X87900070.

Fodor R. V., McKee E. H. and Roisenberg A. (1989) Age distribution of Serra Geral (Paraná) flood basalts, southern Brazil. *J. South Am. Earth Sci.* **2**, 343–349.

Fodor R. V., Sial A. N. and Gandhok G. (2002) Petrology of spinel peridotite xenoliths from northeastern Brazil: Lithosphere with a high geothermal gradient imparted by Fernando de Noronha plume. *J. South Am. Earth Sci.* **15**, 199–214.

Fodor R. V. and Vetter S. K. (1984) Rift-zone magmatism: Petrology of basaltic rocks transitional from CFB to MORB, southeastern Brazil margin. *Contrib. to Mineral. Petrol.* **88**, 307–321.

Garland F., Hawkesworth C. J. and Mantovani M. S. M. (1995) Description and Petrogenesis of the Paraná Rhyolites, Southern Brazil. *J. Petrol.* **36**, 1193–1227.

Gibson S. A., Thompson R. N. and Day J. A. (2006) Timescales and mechanisms of plume-lithosphere interactions: 40Ar/39Ar geochronology and geochemistry of alkaline igneous rocks from the Paraná-Etendeka large igneous province. *Earth Planet. Sci. Lett.* **251**, 1–17.

González-Jiménez J. M., Mondal S. K., Ghosh B., Griffin W. L. and O'Reilly S. Y. (2020) Re-Os Isotope Systematics of Sulfides in Chromitites and Host Lherzolites of the Andaman Ophiolite, India. *Minerals* **10**, 1–21.

Gordon J. M. (1947) Classification of the Gondwanic Rocks of Paraná, Santa Catarina and Rio Grande do Sul. Rio de. *Dept. Nac. Prod. Min., Div. Geol. e Min., Notas Prelim.* **no. 38a**, 1–19.

Griffin W. L., Begg G. C. and O'Reilly S. Y. (2013) Continental-root control on the genesis of magmatic ore deposits. *Nat. Geosci.* **6**, 905–910. Available at: http://dx.doi.org/10.1038/ngeo1954.

Hawkesworth C., Mantovani M. and Peate D. (1988) Lithosphere remobilization during Paraná CFB magmatism. *J. Petrol.* **Special Is**, 205–223.

Hawkesworth C. and Scherstén A. (2007) Mantle plumes and geochemistry. *Chem. Geol.* **241**, 319–331.

Helmy H. M. and Bragagni A. (2017) Platinum-group elements fractionation by selective complexing, the Os, Ir, Ru, Rh-arsenide-sulfide systems above 1020 °C. *Geochim. Cosmochim. Acta* **216**, 169–183. Available at: http://dx.doi.org/10.1016/j.gca.2017.01.040.

Helmy H. M. and Fonseca R. O. C. (2017) The behavior of Pt, Pd, Cu and Ni in the Se-sulfide system between 1050 and 700 ° C and the role of Se in platinum-group elements fractionation in sulfide melts. *Geochim. Cosmochim. Acta*, 0–12. Available at: http://linkinghub.elsevier.com/retrieve/pii/S0016703717302831.

Hill E., Wood B. J. and Blundy J. D. (2000) The effect of Ca-Tschermaks component on trace element partitioning between clinopyroxene and silicate melt. *Lithos* **53**, 203–215.

Holwell D. A., Fiorentini M., McDonald I., Lu Y., Giuliani A., Smith D. J., Keith M. and Locmelis M. (2019) A metasomatized lithospheric mantle control on the metallogenic signature of post-subduction magmatism. *Nat. Commun.* **10**, 1–10. Available at: http://dx.doi.org/10.1038/s41467-019-11065-4.

Holwell D. A. and McDonald I. (2010) A Review of the Behaviour of Platinum Group Elements within Natural Magmatic Sulfide Ore Systems. *Platin. Met. Rev.* **54**, 26–36. Available at: http://openurl.ingenta.com/content/xref?genre=article&issn=0032-1400&volume=54&issue=1&spage=26.

Holzheid A., Sylvester P., O'Neill H., Rubie D. C. and Palme H. (2000) Evidence for a late chondritic veneer in the Earth´s mantle from high pressure partitioning of palladium and platinum. *Nature* **406**, 396–399.

Homrighausen S., Hoernle K., Hauff F., Wartho J.-A., van den Bogaard P. and Garbe-Schönberg D. (2019) New age and geochemical data from the Walvis Ridge: The temporal and spatial diversity of South Atlantic intraplate volcanism and its possible origin. *Geochim. Cosmochim. Acta* **245**, 16–34. Available at: https://linkinghub.elsevier.com/retrieve/pii/S0016703718305076.

Howarth G. H. and Harris C. (2017) Discriminating between pyroxenite and peridotite sources for continental flood basalts (CFB) in southern Africa using olivine chemistry. *Earth Planet. Sci. Lett.* **475**, 143–151. Available at: http://dx.doi.org/10.1016/j.epsl.2017.07.043.

Huber H., Koeberl C., McDonald I. and Reimold W. U. (2001) Geochemistry and petrology of Witwatersrand and dwyka diamictites from south Africa: Search for an extraterrestrial component. *Geochim. Cosmochim. Acta* **65**, 2007–2016.

Hughes H. S. R., McDonald I., Goodenough K. M., Ciborowski T. J. R., Kerr A. C., Davies J. H. F. L. and Selby D. (2014) Enriched lithospheric mantle keel below the Scottish margin of the North Atlantic Craton: Evidence from the Palaeoproterozoic Scourie Dyke Swarm and mantle xenoliths. *Precambrian Res.* **250**, 97–126. Available at: http://dx.doi.org/10.1016/j.precamres.2014.05.026.

Hughes H. S. R., McDonald I. and Kerr A. C. (2015) Platinum-group element signatures in the North Atlantic Igneous Province: Implications for mantle controls on metal budgets during continental breakup. *Lithos* **233**, 89–110. Available at: http://dx.doi.org/10.1016/j.lithos.2015.05.005.

Jellinek A. M. and Manga M. (2004) Links Between Long-lived Hot Spots, Mantle Plumes, D", And Plate Tectonics. *Rev. Geophys.* **42**, 1–35. Available at: http://www.seismo.berkeley.edu/~manga/paper72.pdf.

Jerram D. A. and Widdowson M. (2005) The anatomy of Continental Flood Basalt Provinces: Geological constraints on the processes and products of flood volcanism. *Lithos* **79**, 385–405.

Johnson K. T. M. (1998) Experimental determination of partition coefficients for rare earth and high-field-strength elements between clinopyroxene, garnet, and basaltic melt at high pressures. *Contrib. to Mineral. Petrol.* **133**, 60–68.

Jourdan F., Bertrand H., Schärer U., Blichert-Toft J., Féraud G. and Kampunzu A. B. (2007) Major and trace element and Sr, Nd, Hf, and Pb isotope compositions of the Karoo large igneous province, Botswana - Zimbabwe: Lithosphere vs Mantle Plume Contribution. *J. Petrol.* **48**, 1043–1077.

Keays R. R., Nickel E. H., Groves D. I. and McGoldrick P. J. (1982) Iridium and Palladium as Discriminants of Volcanic-Exhalative, Hydrothermal, and Magmatic Nickel Sulfide Mineralization. *Econ. Geol.* **77**, 1535–1547.

Kent R. Y. W. and Fitton J. G. (2000) Mantle Sources and Melting Dynamics in the British Palaeogene Igneous Province. *J. Petrol.* **41**, 1023–1040.

Kerr A. C. (1997) The geochemistry and significance of plugs intruding the Tertiary Mull-Morvern lava succession, western Scotland. *Scottish J. Geol.* **33**, 157–167.

Kerr A. C. (1995) The geochemistry of the Mull-Morvern Tertiary lava succession, NW Scotland: an assessment of mantle sources during plume-related volcanism. *Chem. Geol.* **122**, 43–58.

Kinzler R. J. (1997) Melting of mantle peridotite at pressures approaching the spinel to garnet transition: Application to mid-ocean ridge basalt petrogenesis. *J. Geophys. Res. B Solid Earth* **102**, 853–874.

Klemme S. (2004) The influence of Cr on the garnet-spinel transition in the Earth's mantle: Experiments in the system MgO-Cr2O3-SiO2 and thermodynamic modelling. *Lithos* **77**, 639–646.

Klemme S. and O'Neill H. S. C. (2000) The near-solidus transition from garnet lherzolite to spinel lherzolite. *Contrib. to Mineral. Petrol.* **138**, 237–248.

Kystol J. and Larsen L. M. (1999) *Analytical procedures in the Rock Geochemical Laboratory of the Geological Survey of Denmark and Greenland.*,

Large R. R., Gemmell J. B., Paulick H. and Huston D. L. (2001) The alteration box plot: A simple approach to understanding the relationship between alteration mineralogy and lithogeochemistry associated with volcanic-hosted massive sulfide deposits. *Econ. Geol. Geol.* **96**, 957–971.

Leinz V. (1949) Contribuição à Geologia dos Derrames Basálticos do Sul do Brasil. *Bol. da Fac. Filos. Ciências e Let. Univ. São Paulo. Geol.*, 1. Available at: http://www.revistas.usp.br/bffcluspgeologia/article/view/121703.

Leinz V., Bartorelli A., Sadowski G. R. and Isotta C. A. L. (1966) Sobre o comportamento do trapp basaltico da Bacia do Paraná. *Bol. da Soc. Bras. Geol.* **15**, 79–91.

Li M. and Zhong S. (2017) The source location of mantle plumes from 3D spherical models of mantle convection. *Earth Planet. Sci. Lett.* **478**, 47–57. Available at: http://linkinghub.elsevier.com/retrieve/pii/S0012821X17304806.

Licht O. A. B. (2018) A revised chemo-chrono-stratigraphic 4-D model for the extrusive rocks of the Paraná Igneous Province. *J. Volcanol. Geotherm. Res.* **355**, 32–54. Available at: https://doi.org/10.1016/j.jvolgeores.2016.12.003.

Lightfoot P. C., Hawkesworth C. J., Hergt J., Naldrett A. J., Gorbachev N. S., Fedorenko V. A. and Doherty W. (1993) Remobilisation of the continental lithosphere by a mantle plume: from picritic and tholeiitic iavas of the Noril'sk District, Siberian Trap, Russia. *Contrib. to Mineral.*

Petrol. **114**, 171–188.

Lightfoot P. C., Hawkesworth C. J., Olshefsky K., Green T., Doherty W. and Keays R. R. (1997) Geochemistry of Tertiary tholeiites and picrites from Qeqertarssuaq (Disko Island) and Nuussuaq, West Greenland with implications for the mineral potential of comagmatic intrusions. *Contrib. to Mineral. Petrol.* **128**, 139–163.

Lindsay J. J., Hughes H. S. R., Yeomans C. M., Andersen J. C. Ø. and McDonald I. (2020) A Machine Learning approach for regional geochemical data: Platinum-Group Element geochemistry vs geodynamic settings of the North Atlantic Igneous Province. *Geosci. Front.* **In Press**. Available at: https://doi.org/10.1016/j.gsf.2020.10.005.

Liu X., Xiong X., Audétat A., Li Y., Song M., Li L., Sun W. and Ding X. (2014) Partitioning of copper between olivine, orthopyroxene, clinopyroxene, spinel, garnet and silicate melts at upper mantle conditions. *Geochim. Cosmochim. Acta* **125**, 1–22.

Lorand J. P. and Luguet A. (2016) Chalcophile and siderophile elements in mantle rocks: Trace elements controlled by trace minerals. *Rev. Mineral. Geochemistry* **81**, 441–488. Available at: http://rimg.geoscienceworld.org/lookup/doi/10.2138/rmg.2016.81.08.

Lorand J. P., Luguet A. and Alard O. (2013) Platinum-group element systematics and petrogenetic processing of the continental upper mantle: A review. *Lithos* **164–167**, 2–21. Available at: http://dx.doi.org/10.1016/j.lithos.2012.08.017.

Lorand J. P., Reisberg L. and Bedini R. M. (2003) Platinum-group elements and melt percolation processes in Sidamo spinel peridotite xenoliths, Ethiopia, East African Rift. *Chem. Geol.* **196**, 57–75.

Maier W. D., Barnes S. J. and Marsh J. S. (2003) The concentrations of the noble metals in Southern African flood-type basalts and MORB: Implications for petrogenesis and magmatic sulphide exploration. *Contrib. to Mineral. Petrol.* **146**, 44–61.

Maier W. D. and Groves D. I. (2011) Temporal and spatial controls on the formation of magmatic PGE and Ni-Cu deposits. *Miner. Depos.* **46**, 841–857.

Maier W. D., Peltonen P., McDonald I., Barnes S. J., Barnes S. J., Hatton C. and Viljoen F. (2012) The concentration of platinum-group elements and gold in southern African and Karelian kimberlite-hosted mantle xenoliths: Implications for the noble metal content of the Earth's mantle. *Chem. Geol.* **302–303**, 119–135. Available at: http://dx.doi.org/10.1016/j.chemgeo.2011.06.014.

Marques L. S., De Min A., Rocha-Júnior E. R. V, Babinski M., Bellieni G. and Figueiredo A. M. G. (2018) Elemental and Sr-Nd-Pb isotope geochemistry of the Florianópolis Dyke Swarm (Paraná Magmatic Province): crustal contamination and mantle source constraints. *J. Volcanol. Geotherm. Res.* **355**, 149–164. Available at: https://doi.org/10.1016/j.jvolgeores.2017.07.005.

Martins-Ferreira M. A. C., Dias A. N. C., Chemale F. and Campos J. E. G. (2020) Intracontinental uplift of the Brazilian Central Plateau linked to continental breakup, orogenies, and basin filling, supported by apatite and zircon fission-track data. *Arab. J. Geosci.* **13**.

McDonald I., Hughes H. S. R., Butler I. B., Harris J. W. and Muir D. (2017) Homogenisation of sulphide inclusions within diamonds: A new approach to diamond inclusion geochemistry. *Geochim. Cosmochim. Acta* **216**, 335–357. Available at: http://dx.doi.org/10.1016/j.gca.2017.04.039.

McDonald I. and Viljoen K. S. (2006) Platinum-group element geochemistry of mantle eclogites: a reconnaissance study of xenoliths from the Orapa kimberlite, Botswana. *Appl. Earth Sci.* **115**, 81–93. Available at: http://www.tandfonline.com/doi/full/10.1179/174327506X138904.

McDonough W. F. and Sun S. S. (1995) The composition of Earth. *Chem. Geol.* **120**, 223–253.

McDonough W. F., Sun S. S., Ringwood A. E., Jagoutz E. and Hofmann A. W. (1992) Potassium, rubidium, and cesium in the Earth and Moon and the evolution of the mantle of the Earth. *Geochim. Cosmochim. Acta* **56**, 1001–1012.

McKenzie D. and White R. (1989) Magmatism at rift zones: The generation of volcanic continental margins and flood basalts. *J. Geophys. Res.* **94**, 7685–7729.

Milholland C. S. and Presnall D. C. (1998) Liquidus phase relations in the CaO-MgO-Al2O3-SiO2 system at 3·0 GPa: The aluminous pyroxene thermal divide and high-pressure fractionation of picritic and komatiitic magmas. *J. Petrol.* **39**, 3–27.

Milner S. C., Duncan A. R., Whittingham A. M. and Ewart A. (1995) Trans-Atlantic correlation of eruptive sequences and individual silicic volcanic units within the Paraná-Etendeka igneous province. *J. Volcanol. Geotherm. Res.* **69**, 137–157.

De Min A., Callegaro S., Marzoli A., Nardy A. J., Chiaradia M., Marques L. S. and Gabbarrini I. (2017) Insights into the petrogenesis of low- and high-Ti basalts: Stratigraphy and geochemistry of four lava sequences from the central Paraná basin. *J. Volcanol. Geotherm. Res.* **355**, 232–252. Available at: https://doi.org/10.1016/j.jvolgeores.2017.08.009.

Mitchell R. H. and Keays R. R. (1981) Abundance and distribution of gold, palladium and iridium in some spinel and garnet lherzolites: implications for the nature and origin of precious metal-rich intergranular components in the upper mantle. *Geochim. Cosmochim. Acta* **45**, 2425–2442.

Momme P., Óskarsson N. and Keays R. R. (2003) Platinum-group elements in the Icelandic rift system: melting processes and mantle sources beneath Iceland. *Chem. Geol.* **196**, 209–234. Available at: https://linkinghub.elsevier.com/retrieve/pii/S000925410200414X.

Momme P., Tegner C., Brooks C. K. and Keays R. R. (2002) The behaviour of platinum-group elements in basalts from the East Greenland rifted margin. *Contrib. to Mineral. Petrol.* **143**, 133–153.

Momme P., Tegner C., Brooks C. K. and Keays R. R. (2006) Two melting regimes during Paleogene flood basalt generation in East Greenland: combined REE and PGE modelling. *Contrib. to Mineral. Petrol.* **151**, 88–100. Available at: http://link.springer.com/10.1007/s00410-005-0047-2.

Morgan W. J. (1971) Convection plumes in the lower mantle. *Nature* **230**, 42–43.

Morgan W. J. (1972) Deep Mantle Convection Plumes and Plate Motions. *Am. Assoc. Pet. Geol. Bull.* **56**, 203–213.

Mungall J. and Brenan J. (2014) Partitioning of platinum-group elements and Au between sulfide liquid and basalt and the origins of mantle-crust fractionation of the chalcophile elements. *Geochim. Cosmochim. Acta* **125**, 265–289. Available at: http://dx.doi.org/10.1016/j.gca.2013.10.002.

Mungall J. E., Andrews D. R. A., Cabri L. J., Sylvester P. J. and Tubrett M. (2005) Partitioning of Cu, Ni, Au, and platinum-group elements between monosulfide solid solution and sulfide melt under controlled oxygen and sulfur fugacities. *Geochim. Cosmochim. Acta* **69**, 4349–4360.

Naldrett A. J. (1997) Key factors in the genesis of Noril'sk, Sudbury, Jinchuan, Voisey's Bay and other world-class Ni-Cu-PGE deposits: implications for exploration. *Aust. J. Earth Sci.*, 283–315.

Natali C., Beccaluva L., Bianchini G., Ellam R. M., Savo A., Siena F. and Stuart F. M. (2016) High-MgO lavas associated to CFB as indicators of plume-related thermochemical effects: The case of ultra-titaniferous picrite–basalt from the Northern Ethiopian–Yemeni Plateau. *Gondwana Res.*

34, 29–48. Available at: https://linkinghub.elsevier.com/retrieve/pii/S1342937X16300302.

Natali C., Beccaluva L., Bianchini G. and Siena F. (2017) Comparison among Ethiopia-Yemen, Deccan, and Karoo continental flood basalts of central Gondwana: Insights on lithosphere versus asthenosphere contributions in compositionally zoned magmatic provinces. *Spec. Pap. Geol. Soc. Am.* **526**, 191–215.

O'Connor J. M. and Duncan R. A. (1990) Evolution of the Walvis Ridge-Rio Grande Rise Hot Spot System: Implications for African and South American Plate motions over plumes. *J. Geophys. Res.* **95**, 17475. Available at: http://doi.wiley.com/10.1029/JB095iB11p17475.

O'Connor J. M. and Jokat W. (2015) Tracking the Tristan-Gough mantle plume using discrete chains of intraplate volcanic centers buried in the Walvis Ridge. *Geology* **43**, 715–718.

Park J. W., Kamenetsky V., Campbell I., Park G., Hanski E. and Pushkarev E. (2017) Empirical constraints on partitioning of platinum group elements between Cr-spinel and primitive terrestrial magmas. *Geochim. Cosmochim. Acta* **216**, 393–416. Available at: http://dx.doi.org/10.1016/j.gca.2017.05.039.

Peach C. L., Mathez E. A. and Keays R. R. (1990) Sulfide melt-silicate melt distribution coefficients for noble metals and other chalcophile elements as deduced from MORB: Implications for partial melting. *Geochim. Cosmochim. Acta* **54**, 3379–3389.

Peach C. L., Mathez E. A., Keays R. R. and Reeves S. J. (1994) Experimentally determined sulfide melt-silicate melt partition coefficients for iridium and palladium. *Chem. Geol.* **117**, 361–377.

Peate D. W. (1997) The Paraná-Etendeka province. *Geophys. Monogr. Ser. Ser* **100**, 217–245.

Peate D. W. and Hawkesworth C. J. (1996) Lithospheric to asthenospheric transition in low-Ti flood basalts from southern Paraná, Brazil. *Chem. Geol.* **127**, 1–24.

Peate D. W., Hawkesworth C. J., Mantovani M. M. S., Rogers N. W. and Turner S. P. (1999) Petrogenesis and stratigraphy of the high-Ti/Y Urubici magma type in the Parana Flood Basalt Province and implications for the nature of 'Dupal'-type mantle in the South Atlantic Region. *J. Petrol.* **40**, 451–473.

Peate D. W., Hawkesworth C. J. and Mantovani M. S. M. (1992) Chemical stratigraphy of the Paraná lavas (South America): classification of magma types and their spatial distribution. *Bull. Volcanol.* **55**, 119–139.

Peate D. W., Hawkesworth C. J., Mantovani M. S. M. and Shukowsky W. (1990) Mantle plumes and flood-basalt stratigraphy in the Parana, South America. *Geology* **18**, 1223–1226.

Philipp H., Eckhardt J.-D. and Puchelt H. (2001) Platinum-Group Elements (PGE) in Basalts of the Seaward-Dipping Reflector Sequence, SE Greenland Coast. *J. Petrol.* **42**, 407–432.

Piccirillo E. M., Melfi A. J., Comin-Chiaramonti P., Bellieni G., Ernesto M., Marques L. S., Nardy A. J. R., Pacca I. G., Roisenberg A. and Stolfa D. (1988) Continental Flood Volcanism From the Paraná Basin (Brazil). In *Continental Flood Basalts* (ed. J. D. McDougall). Kluwer. pp. 195–238.

Pitcher L., Helz R. T., Walker R. J. and Piccoli P. (2009) Fractionation of the platinum-group elments and Re during crystallization of basalt in Kilauea Iki Lava Lake, Hawaii. *Chem. Geol.* **260**, 196–210. Available at: http://dx.doi.org/10.1016/j.chemgeo.2008.12.022.

Polo L. A., Giordano D., Janasi V. A. and Guimarães L. F. (2018) Effusive silicic volcanism in the Paraná Magmatic Province, South Brazil: Physico-chemical conditions of storage and eruption and considerations on the rheological behavior during emplacement. *J. Volcanol. Geotherm. Res.* **355**, 115–135. Available at: https://doi.org/10.1016/j.jvolgeores.2017.05.027.

Powell W. and O'Reilly S. (2007) Metasomatism and sulfide mobility in lithospheric mantle beneath eastern Australia: Implications for mantle Re-Os chronology. *Lithos* **94**, 132–147.

Rämö O. T., Heikkilä P. A. and Pulkkinen A. H. (2016) Geochemistry of Paraná-Etendeka basalts from Misiones, Argentina: Some new insights into the petrogenesis of high-Ti continental flood basalts. *J. South Am. Earth Sci.* **67**, 25–39.

Rehkämper M., Halliday A. N., Barfod D., Fitton J. G. and Dawson J. B. (1997) Platinum-group element abundance patterns in different mantle environments. *Science (80-.).* **278**, 1595–1598.

Renne P. R., Glen J. M., Milner S. C. and Duncan A. R. (1996) Age of Etendeka flood volcanism and associated intrusions in southwestern Africa. *Geology* **24**, 659–662.

Richardson S. H., Erlank A. J., Duncan A. R. and Reid D. L. (1982) Correlated Nd, Sr and Pb isotope variation in Walvis Ridge basalts and implications for the evolution of their mantle source. *Earth Planet. Sci. Lett.* **59**, 327–342.

Rielli A., Tomkins A. G., Nebel O., Raveggi M., Jeon H., Martin L. and Ávila J. N. (2018) Sulfur isotope and PGE systematics of metasomatised mantle wedge. *Earth Planet. Sci. Lett.* **497**, 181–192. Available at: https://doi.org/10.1016/j.epsl.2018.06.012.

Righter K., Campbell A. J., Humayun M. and Hervig R. L. (2004) Partitioning of Ru, Rh, Pd, Re, Ir, and Au between Cr-bearing spinel, olivine, pyroxene and silicate melts. *Geochim. Cosmochim. Acta* **68**, 867–880.

Righter K., Humayun M. and Danielson L. (2008) Partitioning of palladium at high pressures and temperatures during core formation. *Nat. Geosci.* **1**, 321–323.

Rivalenti G., Mazzucchelli M., Girardi V. A. V., Vannucci R., Barbieri M. A., Zanetti A. and Goldstein S. L. (2000) Composition and processes of the mantle lithosphere in northeastern Brazil and Fernando de Noronha: Evidence from mantle xenoliths. *Contrib. to Mineral. Petrol.* **138**, 308–325.

Rocha-Júnior E. R. V, Marques L. S., Babinski M., Nardy A. J. R., Figueiredo A. M. G. and Machado F. B. (2013) Sr-Nd-Pb isotopic constraints on the nature of the mantle sources involved in the genesis of the high-Ti tholeiites from northern Paraná Continental Flood Basalts (Brazil). *J. South Am. Earth Sci.* **46**, 9–25. Available at: http://dx.doi.org/10.1016/j.jsames.2013.04.004.

Rossetti L., Lima E. F., Waichel B. L., Hole M. J., Simões M. S. and Scherer C. M. S. (2018) Lithostratigraphy and volcanology of the Serra Geral Group, Paraná-Etendeka Igneous Province in Southern Brazil: Towards a formal stratigraphical framework. *J. Volcanol. Geotherm. Res.* **355**, 98–114. Available at: https://doi.org/10.1016/j.jvolgeores.2017.05.008.

Saunders A. D., Fitton J. G., Kerr A. C., Norry M. J. and Kent R. W. (1997) The North Atlantic Igneous Province. In *Large Igneous Provinces: Continental, Oceanic and Planetary Flood Volcanism* (eds. J. J. Mahoney and M. . Coffin). American Geophysical Union Monograph. pp. 45–93. Available at: http://doi.wiley.com/10.1029/GM100p0045.

Schmidt G., Witt-Eickschen G., Palme H., Seck H., Spettel B. and Kratz K. L. (2003) Highly siderophile elements (PGE, Re and Au) in mantle xenoliths from the West Eifel volcanic field (Germany). *Chem. Geol.* **196**, 77–105.

Shannon M. C. and Agee C. B. (1998) Percolation of Core Melts at Lower Mantle Conditions. *Sci. New Ser.* **280**, 1059–1061.

Shaw D. M. (1970) Trace element fractionation during anatexis. *Geochim. Cosmochim. Acta* **34**, 237–

243.

Song X. Y., Qi H. W., Robinson P. T., Zhou M. F., Cao Z. M. and Chen L. M. (2008) Melting of the subcontinental lithospheric mantle by the Emeishan mantle plume; evidence from the basal alkaline basalts in Dongchuan, Yunnan, Southwestern China. *Lithos* **100**, 93–111.

Spandler C. and O'Neill H. S. C. (2010) Diffusion and partition coefficients of minor and trace elements in San Carlos olivine at 1,300°C with some geochemical implications. *Contrib. to Mineral. Petrol.* **159**, 1–28.

Stein C. A. and Stein S. S. (1992) A model for the global variation in oceanic depth and heat flow with lithospheric age. *Nature* **359**, 123–129.

Stewart K., Turner S. P., Kelley S., Hawkesworth C., Kirstein L. and Mantovani M. (1996) 3-D, 40Ar-39Ar geochronology in the Paraná continental flood basalt province. *Earth Planet. Sci. Lett.* **143**, 95–109. Available at: http://medcontent.metapress.com/index/A65RM03P4874243N.pdf.

Stracke A., Hofmann A. W. and Hart S. R. (2005) FOZO, HIMU, and the rest of the mantle zoo. *Geochemistry, Geophys. Geosystems* **6**.

Tassara S., González-Jiménez J. M., Reich M., Schilling M. E., Morata D., Begg G., Saunders E., Griffin W. L., O'Reilly S. Y., Grégoire M., Barra F. and Corgne A. (2017) Plume-subduction interaction forms large auriferous provinces. *Nat. Commun.* **8**, 1–7.

Tegner C., Thy P., Holness M. B., Jakobsen J. K. and Lesher C. E. (2009) Differentiation and compaction in the Skaergaard intrusion. *J. Petrol.* **50**, 813–840.

Thompson R. N. and Gibson S. A. (1991) Subcontinental mantle plumes, hotspots and pre-existing thinspots. *J. Geol. Soc. London.* **148**, 973–977. Available at: http://jgs.lyellcollection.org/cgi/doi/10.1144/gsjgs.148.6.0973.

Turner S. P., Hawkesworth C., Gallagher K., Stewart K., Peate D. and Mantovani M. (1996) Mantle plumes, flood basalts, and thermal models for melt generation beneath continents: Assessment of a conductive heating model and application to the Paraná. *J. Geophys. Res. Solid Earth* **101**, 11503–11518. Available at: http://doi.wiley.com/10.1029/96JB00430.

Turner S. P., Peate D. W., Hawkesworth C. J. and Mantovani M. S. M. (1999) Chemical stratigraphy of the Parana basalt succession in western Uruguay: Further evidence for the diachronous nature of the Parana magma types. *J. Geodyn.* **28**, 459–469.

Ussami N., Chaves C. A. M., Marques L. S. and Ernesto M. (2013) Origin of the rio grande Rise-Walvis ridge reviewed integrating palaeogeographic reconstruction, isotope geochemistry and flexural modelling. *Geol. Soc. Spec. Publ.* **369**, 129–146.

Wade C. E., Payne J. L., Barovich K. M. and Reid A. J. (2019) Heterogeneity of the sub-continental lithospheric mantle and 'non-juvenile' mantle additions to a Proterozoic silicic large igneous province. *Lithos* **340–341**, 87–107. Available at: https://doi.org/10.1016/j.lithos.2019.05.005.

Walter M., Katsura T., Kubo A., Shinmei T., Nishikawa O., Ito E., Lesher C. M. and Funakoshi K. (2002) Spinel–garnet lherzolite transition in the system CaO-MgO-Al2O3-SiO2 revisited: an in situ X-ray study. *Geochim. Cosmochim. Acta* **66**, 2109–2121. Available at: http://www.sciencedirect.com/science/article/pii/S0016703702008451.

Wang Z., Cheng H., Zong K., Geng X., Liu Y., Yang J., Wu F., Becker H., Foley S. and Wang C. Y. (2020) Metasomatized lithospheric mantle for Mesozoic giant gold deposits in the North China craton. *Geology* **48**, 169–173.

White R. S. and McKenzie D. (1995) Mantle plumes and flood basalts. *J. Geophys. Res. Solid Earth*

100, 17543–17585. Available at: http://doi.wiley.com/10.1029/95JB01585.

Wildman M., Brown R., Persano C., Beucher R., Stuart F. M., Mackintosh V., Gallagher K., Schwanethal J. and Carter A. (2017) Contrasting Mesozoic evolution across the boundary between on and off craton regions of the South African plateau inferred from apatite fission track and (U-Th-Sm)/He thermochronology. *J. Geophys. Res. Solid Earth* **122**, 1517–1547.

Wilson M. R., Kyser T. K. and Fagan R. (1996) Sulfur isotope systematics and platinum group element behavior in REE-enriched metasomatic fluids: A study of mantle xenoliths from Dish Hill, California, USA. *Geochim. Cosmochim. Acta* **60**, 1933–1942.

de Wit M. J., Stankiewicz J. and Reeves C. (2008) Restoring Pan-African-Brasiliano connections: more Gondwana control, less Trans-Atlantic corruption. *Geol. Soc. London, Spec. Publ.* **294**, 399–412. Available at: http://sp.lyellcollection.org/lookup/doi/10.1144/SP294.20.

Wooden J. L., Czamanske G. K., Fedorenko V. A., Arndt N. T., Chauvel C., Bouse R. M., King B. S. W., Knight R. J. and Siems D. F. (1993) Isotopic and trace-element constraints on mantle and crustal contributions to Siberian continental flood basalts, Noril'sk area, Siberia. *Geochim. Cosmochim. Acta* **57**, 3677–3704.

Woodland S. J., Pearson D. G. and Thirlwall M. F. (2002) A Platinum Group Element and Re–Os Isotope Investigation of Siderophile Element Recycling in Subduction Zones: Comparison of Grenada, Lesser Antilles Arc, and the Izu–Bonin Arc. *J. Petrol.* **43**, 171–198. Available at: http://academic.oup.com/petrology/article/43/1/171/1399902.

Xiao L., Xu Y. G., Mei H. J., Zheng Y. F., He B. and Pirajno F. (2004) Distinct mantle sources of low-Ti and high-Ti basalts from the western Emeishan large igneous province, SW China: Implications for plume-lithosphere interaction. *Earth Planet. Sci. Lett.* **228**, 525–546.

Zhang M., O'Reilly S. Y., Wang K. L., Hronsky J. and Griffin W. L. (2008) Flood basalts and metallogeny: The lithospheric mantle connection. *Earth Sci. Rev.* **86**, 145–174.

Ziberna L., Klemme S. and Nimis P. (2013) Garnet and spinel in fertile and depleted mantle: Insights from thermodynamic modelling. *Contrib. to Mineral. Petrol.* **166**, 411–421.

Zindler A. and Hart S. R. (1986) Chemical Geodynamics. *Ann. Rev. Earth Planet. Sci* **14**, 493–571. Available at: www.annualreviews.org.

Figure Captions -

Figure 1 - a) Schematic map showing the eruption of the Paraná-Etendeka flood basalts over the conjoined South American and African continents (135 Ma) and their current formation with the Rio Grande Rise (RGR), Walvis Ridge (WR) and Tristan-Gough islands (TG) in between. b) Representative summary timeline of eruptive products of the PELIP with incipient rifting. c) Sample map for this study (Paraná region) with High-Ti and Low-Ti provinces and CFB boundaries. Markers denote sample localities – see Supplementary X for further sample details. Representative stratigraphy is given for the north and south with magma-types classified as: north - Pitanga (PN), Paranapanema (PP) and Ribeira (RI); south - Gramado (GR), Esmeralda (ES), Urubici (UR) and Silicic (S), based on (Turner et al., 1999).

Figure 2 - Classification diagrams based on Peate et al. (1992): a) MgO vs. Zr; b) MgO vs. TiO_2; c) Ti/Y vs. Ti/Zr. d) Total Alkali vs. Silica (TAS) petrological/geochemical discriminant diagram for the Serra Geral sample set. Colours refer to Peate classifications and symbols for Licht classifications as per the legend in 2a. Dashed lines for approximate HT/LT division are from Peate (1997). Dashed lines for approximate Type 1 and 4 division (2.85 wt. % TiO_2) from Licht (2018). Arrows refer to approximate development trajectory. In the key, dashes indicate that no data was available for that particular magma-type either in this study (large coloured markers) or the literature (small greyscale markers). Literature database with references is provided in Supplementary A2. S – Southern, C-N – Central-Northern.

Figure 3 - Harker bivariate plots for Serra Geral lavas: MgO vs. a) TiO2, b) Fe2O3, c) Al2O3, d) MnO, e) CaO, f) Na2O, g) K2O, h) P2O5. With fractionation vectors for evolving liquid compositions for Fo – forsterite, Fa – fayalite, Aug – augite, En – enstatite, Diop - diopside, an – anorthite, Al – albite, Sp – spinel, Uv – ulvospinel, Mg – magnetite, Cr – chromite, Ru – rutile, Im – ilmenite, Bi – biotite, Ho – hornblende, KF – K-feldspar. S – Southern, C-N – Central-Northern.

Figure 4 - Bivariate plots for base metal concentrations in Serra Geral lavas: MgO vs. a) Ni, b) Cu, c) Co, d) Cr. With fractionation vectors for evolving liquid compositions for Ol – olivine, Pyx – pyroxene, Sul – sulphide, and Cr – chromite. S – Southern, C-N – Central-Northern.

Figure 5 - Chondrite-normalised (McDonough and Sun, 1995) rare earth element plots for Serra Geral lavas: a) Urubici; b) Pitanga; c) Paranapanema; d) Esmeralda; e) Gramado; f) silicic Palmas and Chapecó. Grey shaded area – Urubici magma-type for reference. S – Southern, C-N – Central-Northern.

Figure 6 - Selection of lithophile and REE ratio discriminant plots for Serra Geral lavas. a) SiO2 vs. Nb/La, b) (Th/Ta)n vs. (Sm/Yb)n; c) (Th/Ta)n vs.(La/Sm)n; d) (Sm/Yb)n vs. (La/Sm)n. (Annotations for

6b and 6c based on Wooden et al., 1993; for 6a and 6d based on Xiao et al., 2004). S – Southern, C-N – Central-Northern.

Figure 7 - Trace element concentrations normalised by Primitive Mantle values (McDonough et al., 1992), arranged according to increasing compatibility, for the Serra Geral lavas: a) Urubici; b) Pitanga; c) Paranapanema; d) Esmeralda; e) Gramado; f) silicic Palmas and Chapecó. Grey shaded area – Urubici magma-type for reference. S – Southern, C-N – Central-Northern.

Figure 8 - Chondrite-normalised (McDonough and Sun, 1995) PGE plots for Serra Geral lavas and locations. a) Urubici; b) Pitanga; c) Paranapanema; d) Esmeralda; e) Gramado; f) Chapecó. Grey shaded area – Urubici magma-type for reference. S – Southern, C-N – Central-Northern.

Figure 9 - PGE Bivariate plots of Serra Geral lavas for MgO vs a) Os, b) Ir, c) Ru, d) Rh, e) Pt and f) Pd. S – Southern, C-N – Central-Northern.

Figure 10 - Bivariate plots for PGE concentrations as ratios for Serra Geral lavas. a) Pd vs. (Cu/Pd)*1000; b) Ir vs. Pd/Ir with vectors for incompatible fractionation and olivine accumulation, and markers for Primitive Upper Mantle and Skaergaard compositions from Hughes et al. (2015); c) Pd/Ir vs. Ti/Y; d) Ru/Pd vs. (Sm/Yb)n. Literature data used in 10a and 10b from: Lightfoot et al. (1997); Philipp et al. (2001); Momme et al. (2002); Momme et al. (2003); Hughes et al. (2015).

Figure 11 - Bivariate plots of a) Rh/Pd vs. Rh/Ir and b) Ru/Pd vs. Ru/Rh, demonstrating the differences between the Serra Geral lava PGE ratios, with comparison data for intraplate xenoliths (Maier et al., 2012), Iceland (Momme et al., 2003) and Cameroon pyroxenites (Abeng et al., 2012)

Figure 12 – Melt modelling for Serra Geral magma PGE and Au concentrations based on the parameters from Table 2. a) Arc xenolith starting compositions, representing Type 1 (Central-Northern) magma generation. Metasomatised mantle sources can produce the characteristic Pt-Pd-Au enrichment in the corresponding Paranapanema samples at ~20 % partial melting. b) Cratonic and off-cratonic xenolith starting compositions, representing Type 1 (Southern) magma generation. Magma produced at 20 % partial melting (i.e. sulphides exhausted) releases PGE to roughly the chondrite-normalised concentrations in Gramado and Esmeralda samples, but the Ru-Rh 'hump' is not achieved until spinel is also exhausted (25 % partial melting).

Figure 13 – Metallogenic model for the Serra Geral flood basalts and their parent magmas based on geochemical interpretations, literature information and modelling (Fig. 11). Thinner lithosphere above the Tristan plume, either situated nearer to the future Atlantic rift (ie. south-east Paraná and Etendeka) or from progressive craton extension (i.e. north-west Paraná) promotes higher degrees of

partial melting at shallower depths. Type 4 magmas diversify mainly by partial melt extraction and fractional crystallisation (FC) from a plume-proximal source with minimal crustal contamination. Type 1 (Central-Northern) magmas, generated when the HT source begins melting in shallow SCLM regions (F = 0.2), incorporate Pd, Au and Cu from metasomatic sulphides. Type 1 (Southern) lavas diversify by assimilation and fraction crystallisation (AFC), and mafic varieties contain elevated Ru and Rh content via higher degree melts (F = 0.25) of SCLM spinel and sulphides. Based on work by Beccaluva et al. (2020); Rämö et al. (2016); Turner et al. (1999). S – Southern, C-N – Central-Northern.

Table Captions –

Table 1 – Summary of geochemical classification schemes used in this study (Peate et al., 1992 and Licht, 2018). The classification criteria for Peate et al. (1992) is referred to in Figure 2, whilst the geochemical concentrations used for the sixteen types in Licht (2018) are given in this table along with a rough proportion of the total Serra Geral volume. Gra – Gramado, Esm – Esmeralda, Par – Paranapanema.

Table 1 – Parameters used in melting models. [a] Spinel peridotite melt modes from Johnson (1998) and Kinzler (1997), with addition of sulphide. [b] D-values for olivine from Brenan et al. (2003) and Spandler and O'Neill (2010). [c] D-values for orthopyroxene from Beattie et al., (1991) and Liu et al. (2014). [d] D-values for clinopyroxene from Hill et al. (2000) and Righter et al. (2004). [e] D-values for spinel from Liu et al. (2014), Park et al. (2017) and Righter et al. (2004). [f] D-values for sulphide from Mungall and Brenan (2014). [g] Arc xenolith concentrations from Wilson et al. (1996). [h] Craton xenolith concentrations from Maier et al. (2012). [I] Off-craton xenolith concentrations from Schmidt et al. (2003). Italicised values were unavailable in the literature for silicates, but assigned neutral values based on olivine values, given their lesser significance to melt composition compared to spinel and sulphide.

Supplementary Items –

Supplementary A1 - Sample data base for Serra Geral samples collected for this study including sample localities, properties and hand specimen descriptions.

Supplementary A2 – Literature data base used in Figure 2, including full references

Supplementary B – Raw bulk geochemical data for major (XRF), trace (ICP-MS) and PGE-Au (fire assay), produced directly from labs. Includes standard measurements, instrument details, duplicates, and (for PGE-Au) detection limits.

Supplementary C – Merged bulk geochemical data sheet used in all further analyses, including classifications via Peate et al. (1992) and Licht (2018) schemes and various ratios.

Supplementary D - Bivariate plots for alteration indicators in Serra Geral lavas. a) MgO vs. Loss-On-Ignition (LOI); b) Alteration Index vs. Chlorite-Carbonate-Pyrite (CCP) Index. Alteration vectors and 'least alteration box' from Large et al. (2001).

Supplementary E – Modelling sheets for Figure 11. Includes full working calculations, plots and all parameters used in modelling. Discussed fully in Section 4.2.3 of article.

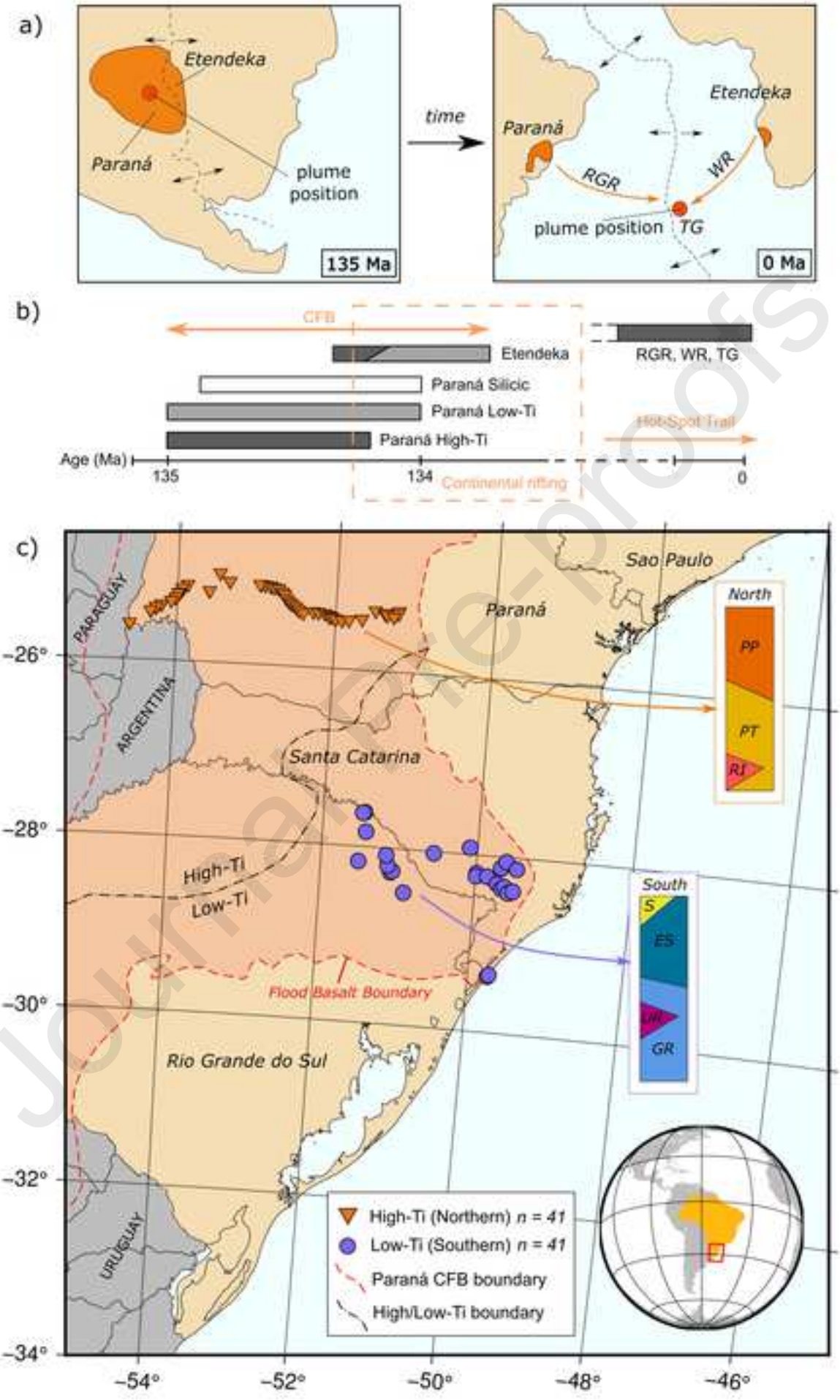
a)
Etendeka
Paraná
plume position
135 Ma
time
Paraná
Etendeka
RGR
WR
plume position
TG
0 Ma
b)
CFB
Etendeka
RGR, WR, TG
Paraná Silicic
Paraná Low-Ti
Paraná High-Ti
HotSpot Trail
Age (Ma)
135
134
Continental rifting
0
c)
Sao Paulo
Paraná
PARAGUAY
ARGENTINA
Santa Catarina
High-Ti
Low-Ti
Flood Basalt Boundary
Rio Grande do Sul
URUGUAY
North
PP
PT
RI
South
S
ES
LH
GR
High-Ti (Northern) n = 41
Low-Ti (Southern) n = 41
Paraná CFB boundary
High/Low-Ti boundary
−26°
−28°
−30°
−32°
−34°
−54°
−52°
−50°
−48°
−46°

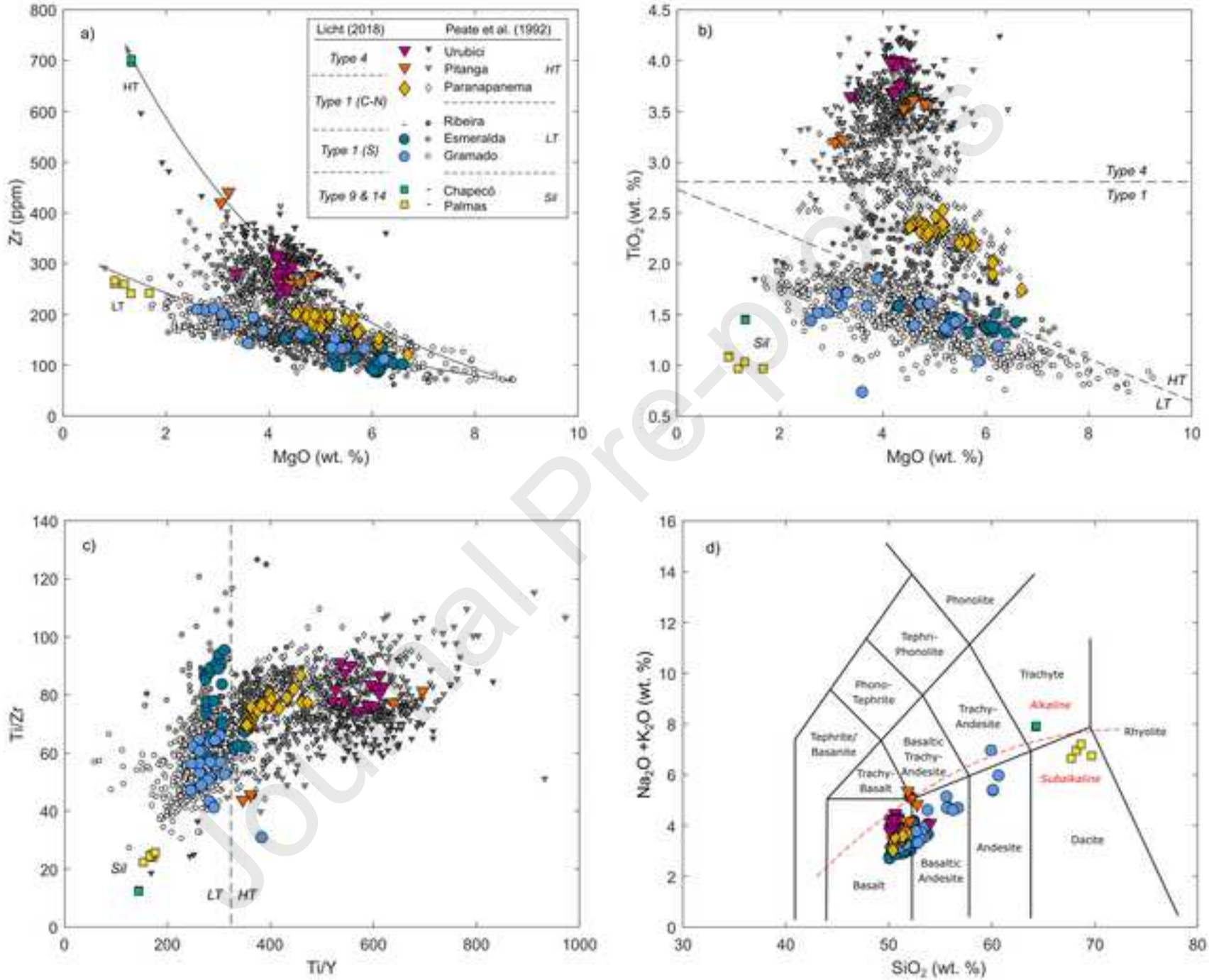

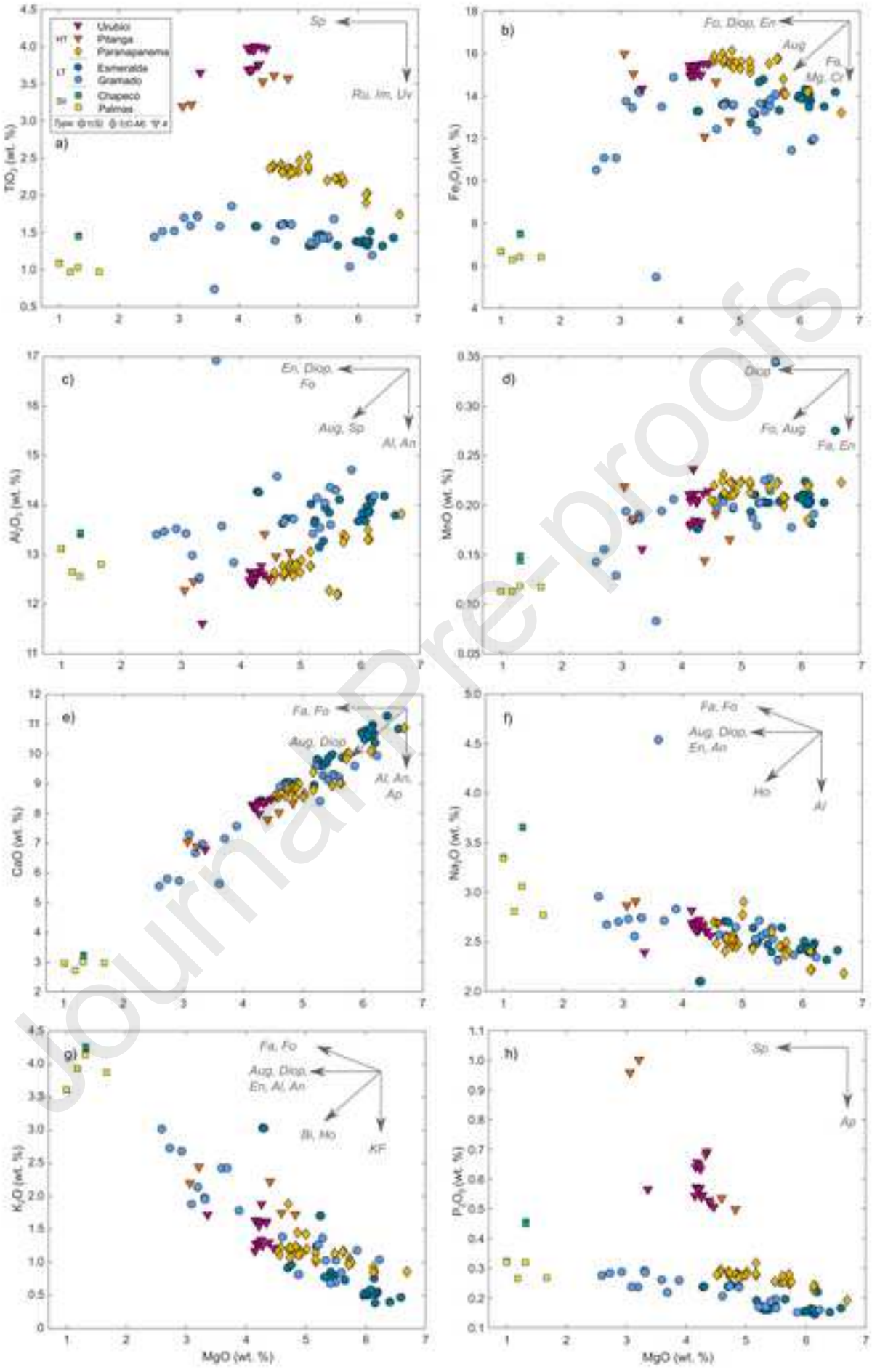

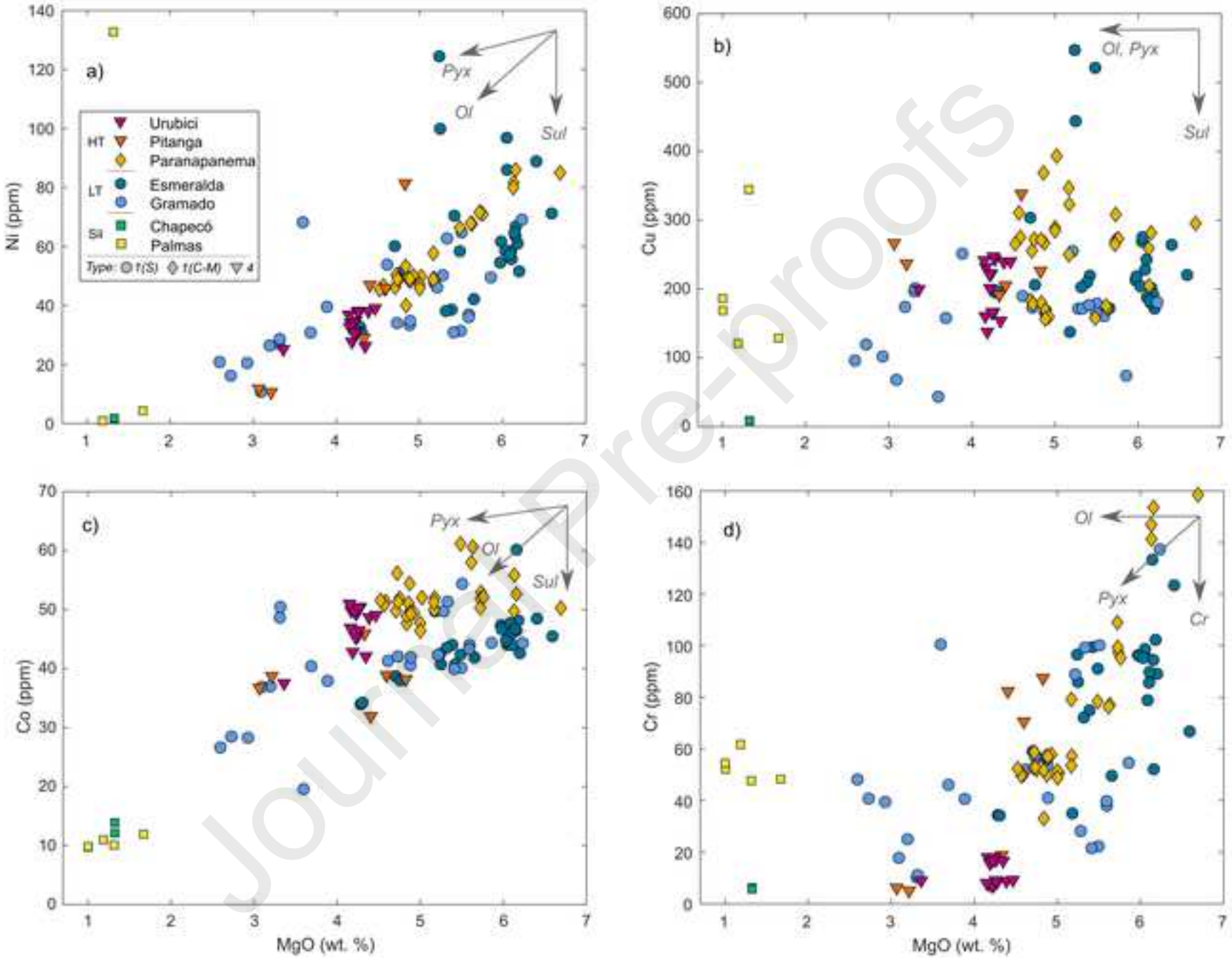

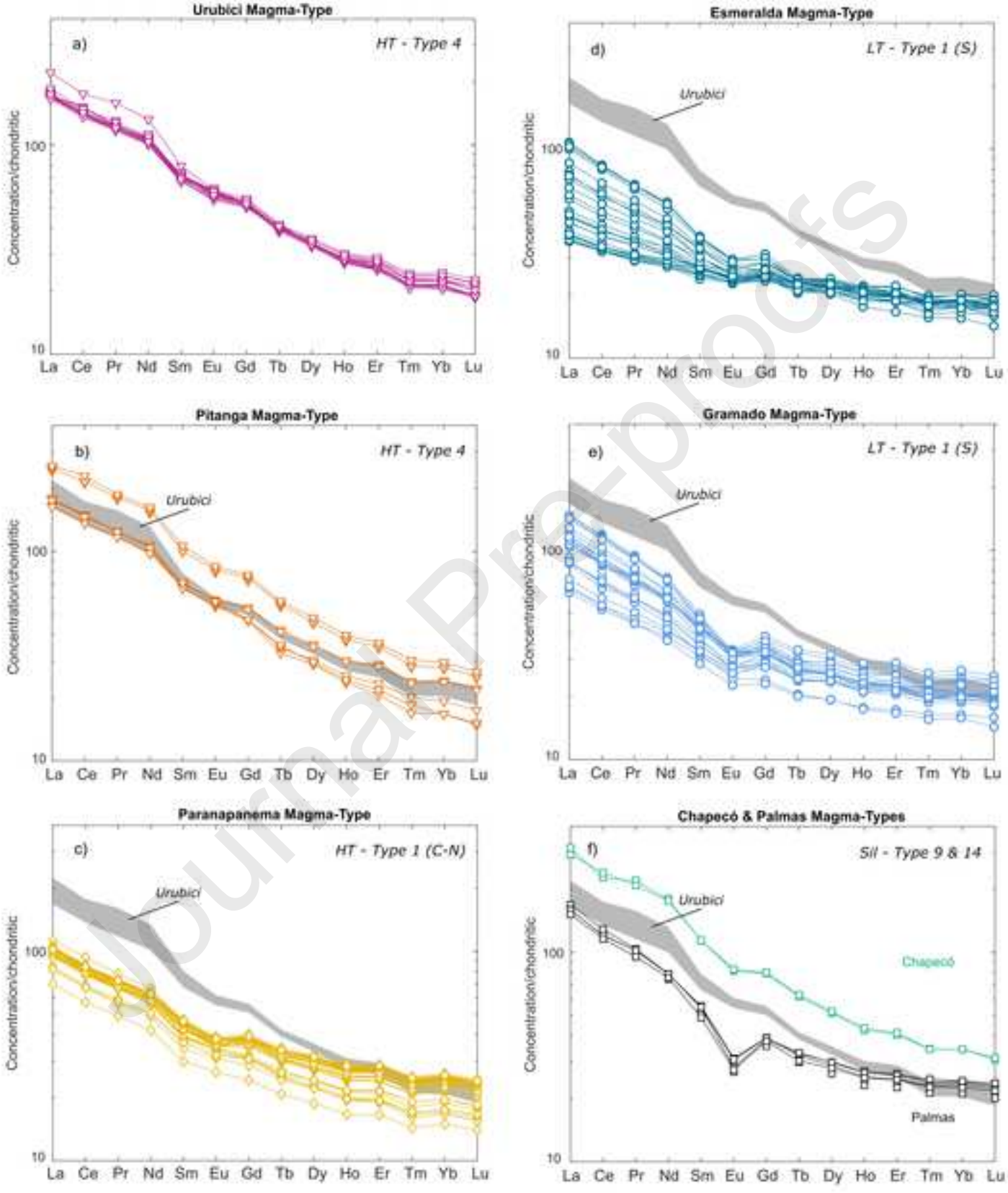

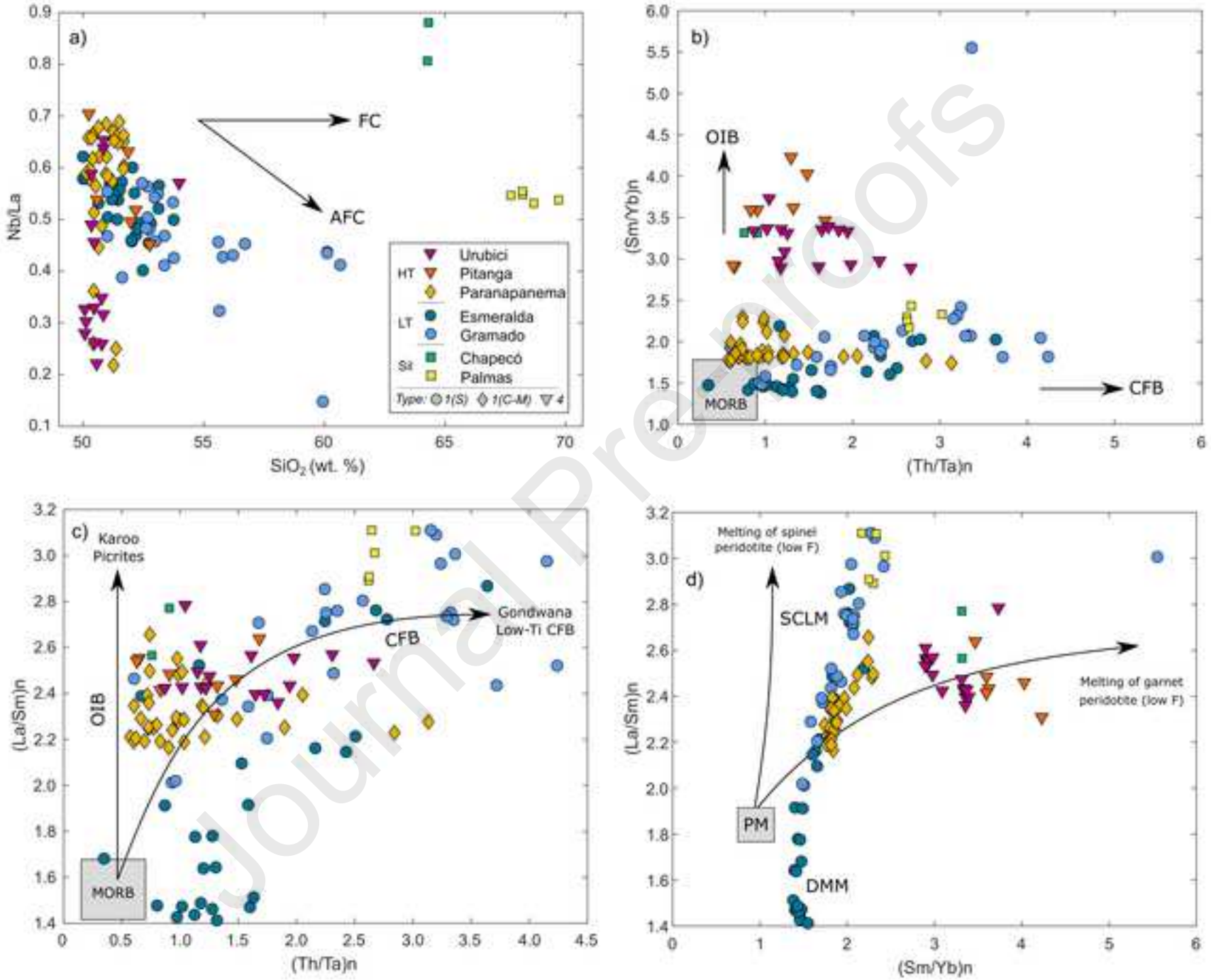

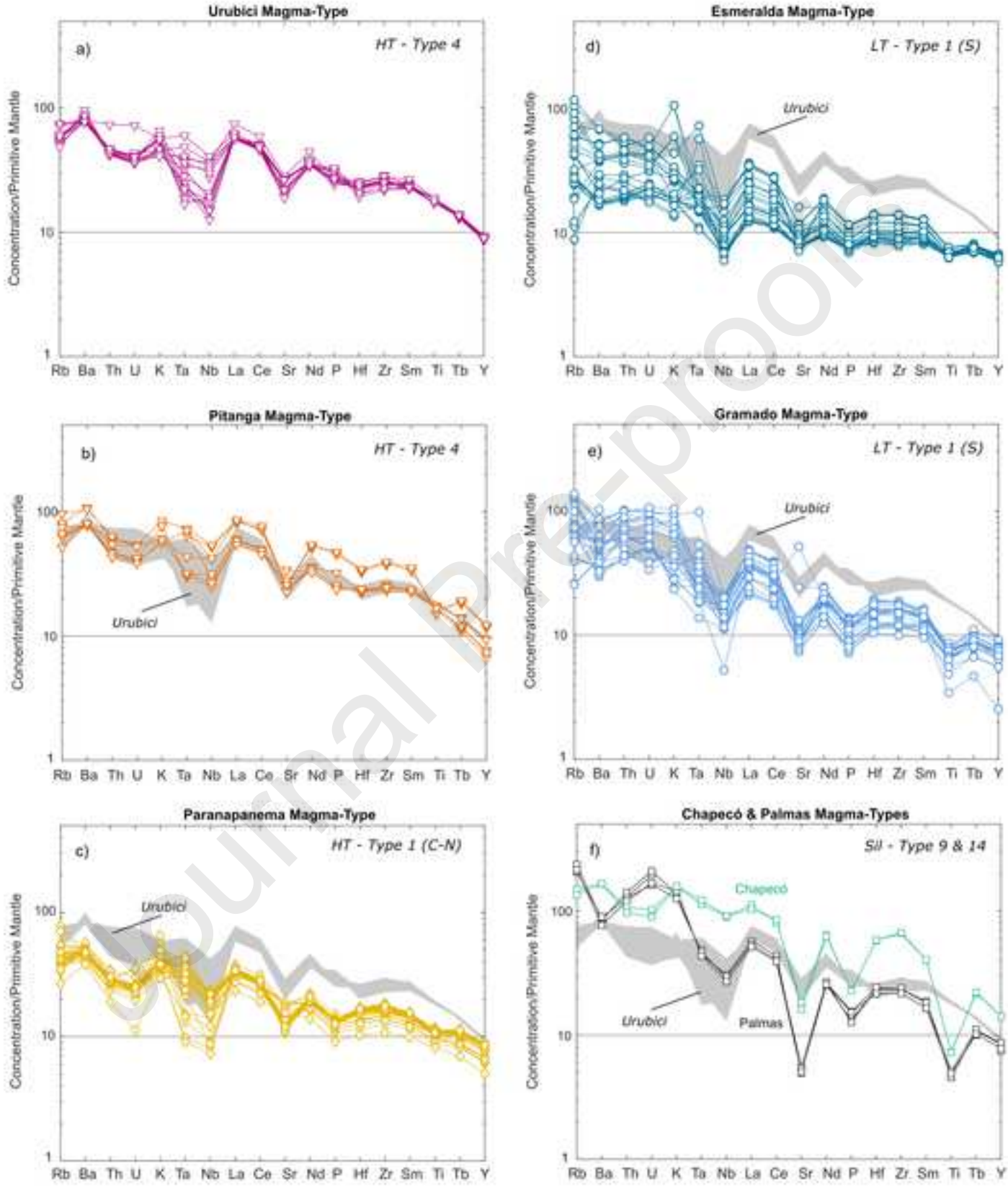

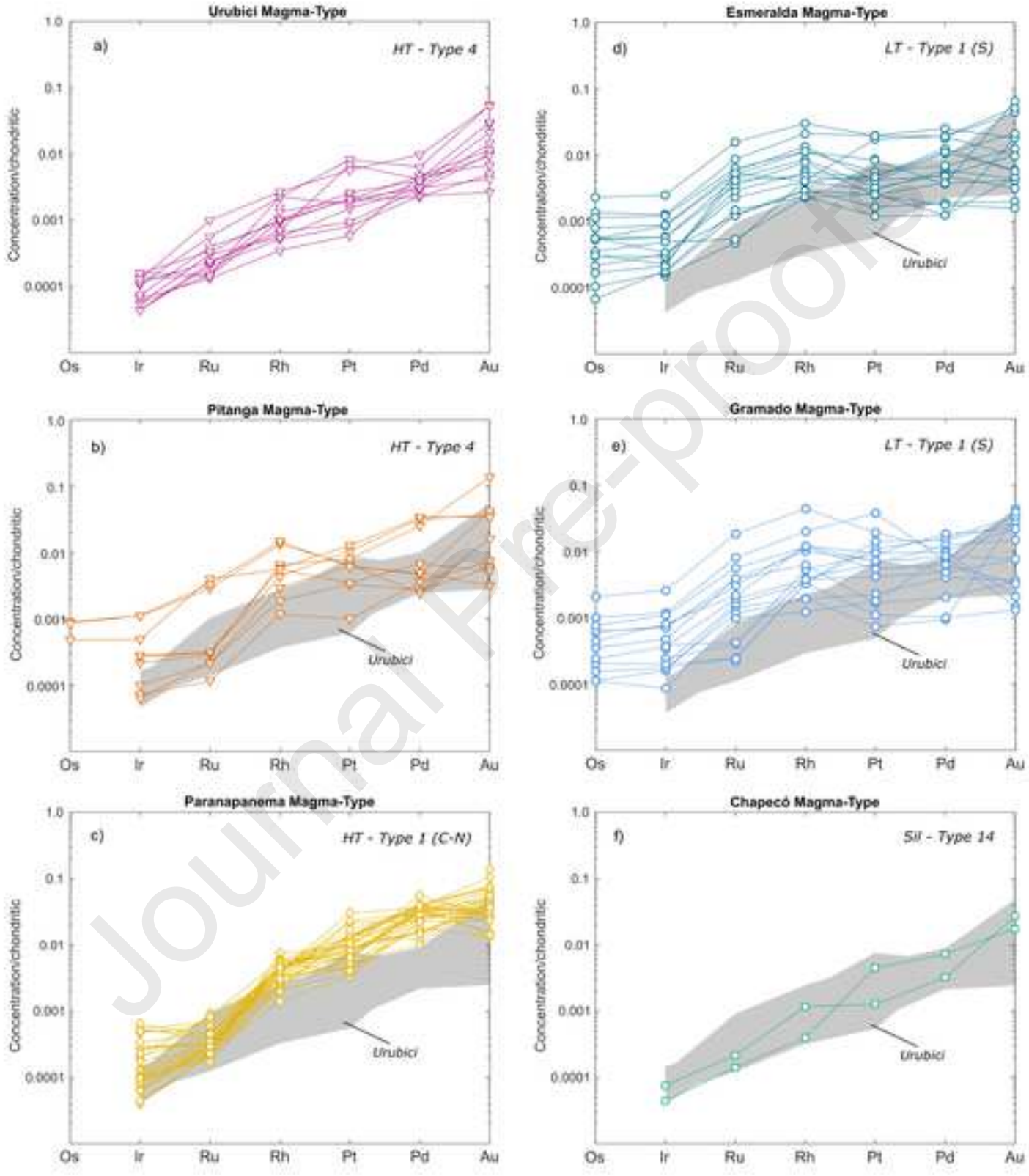

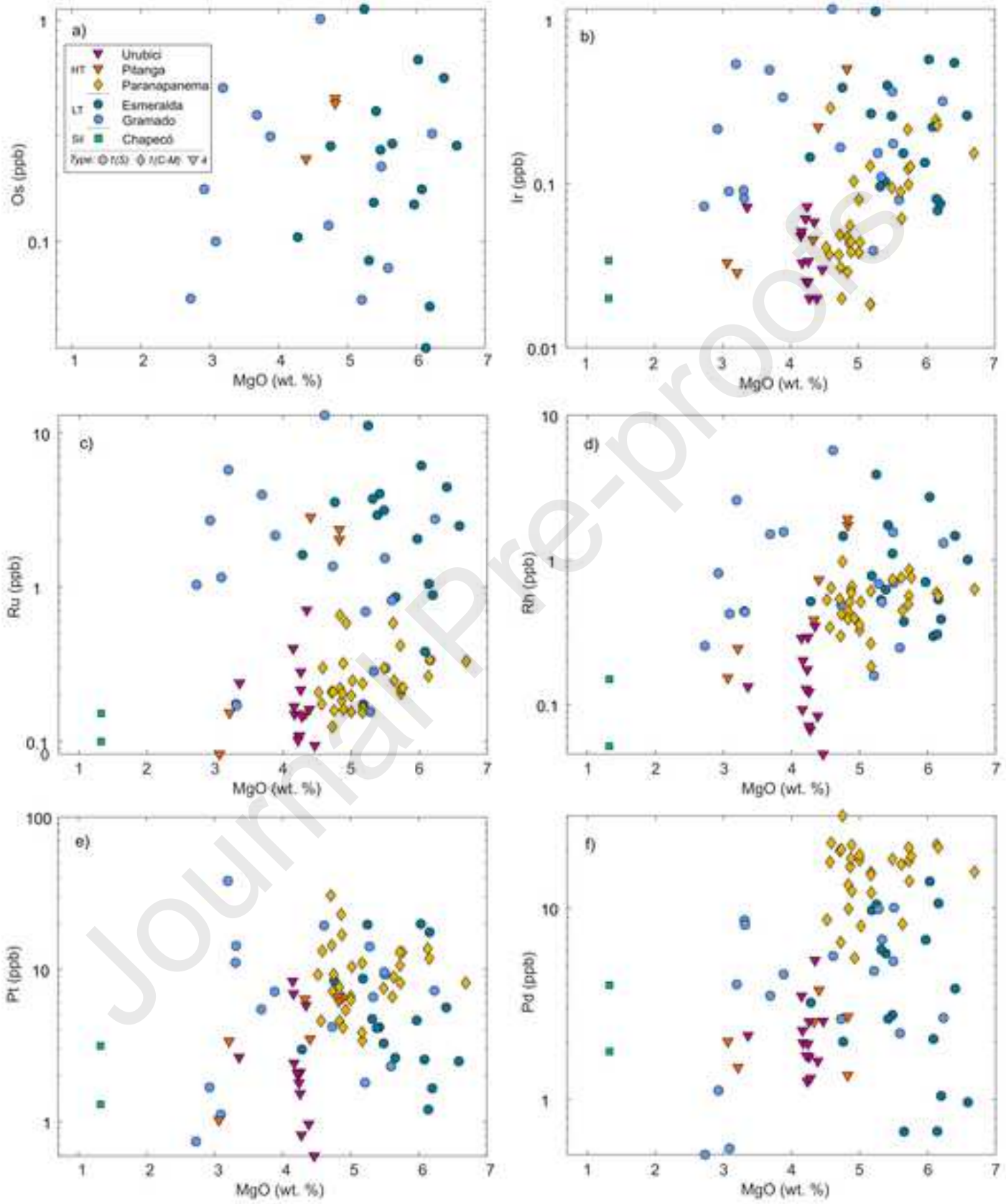

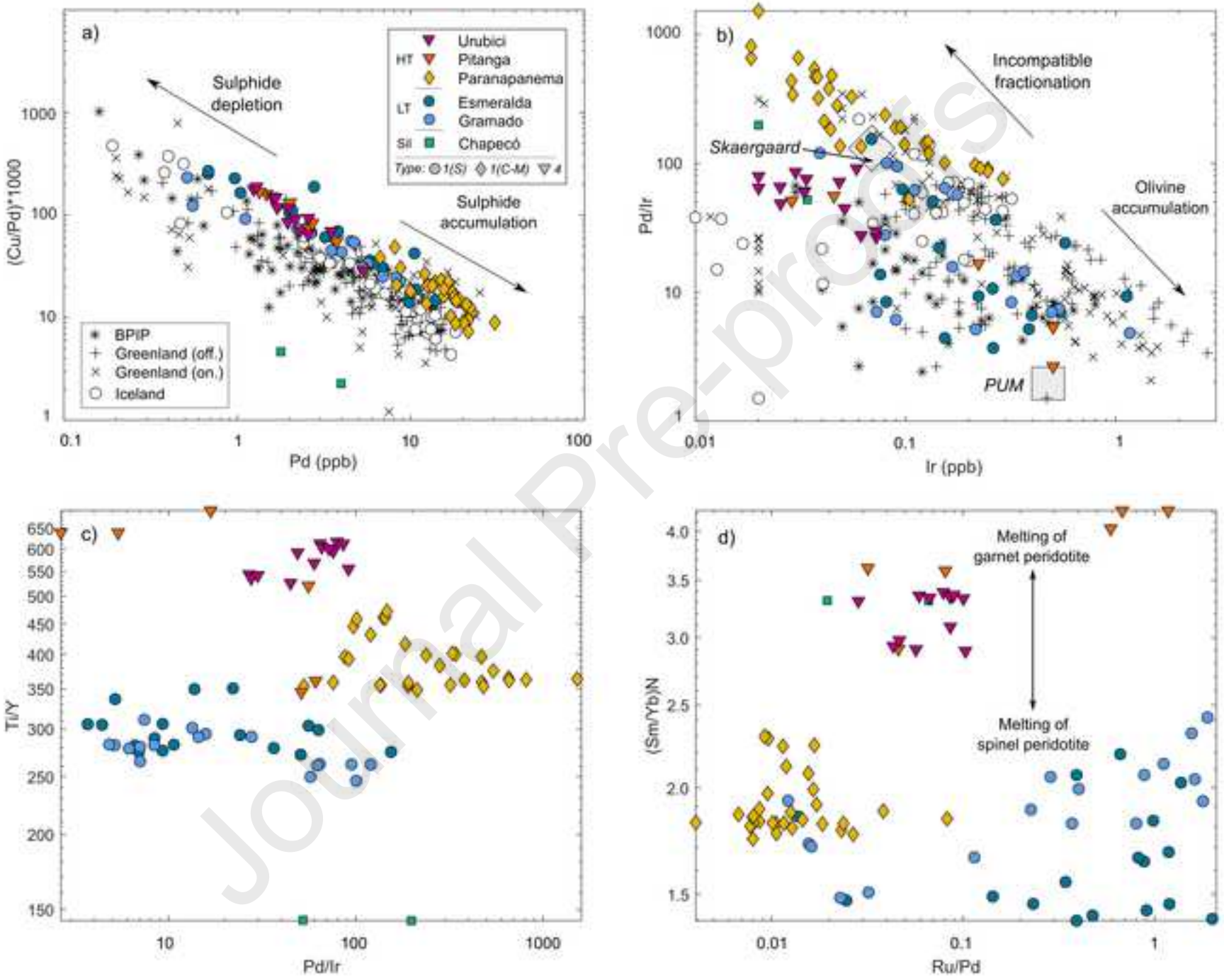

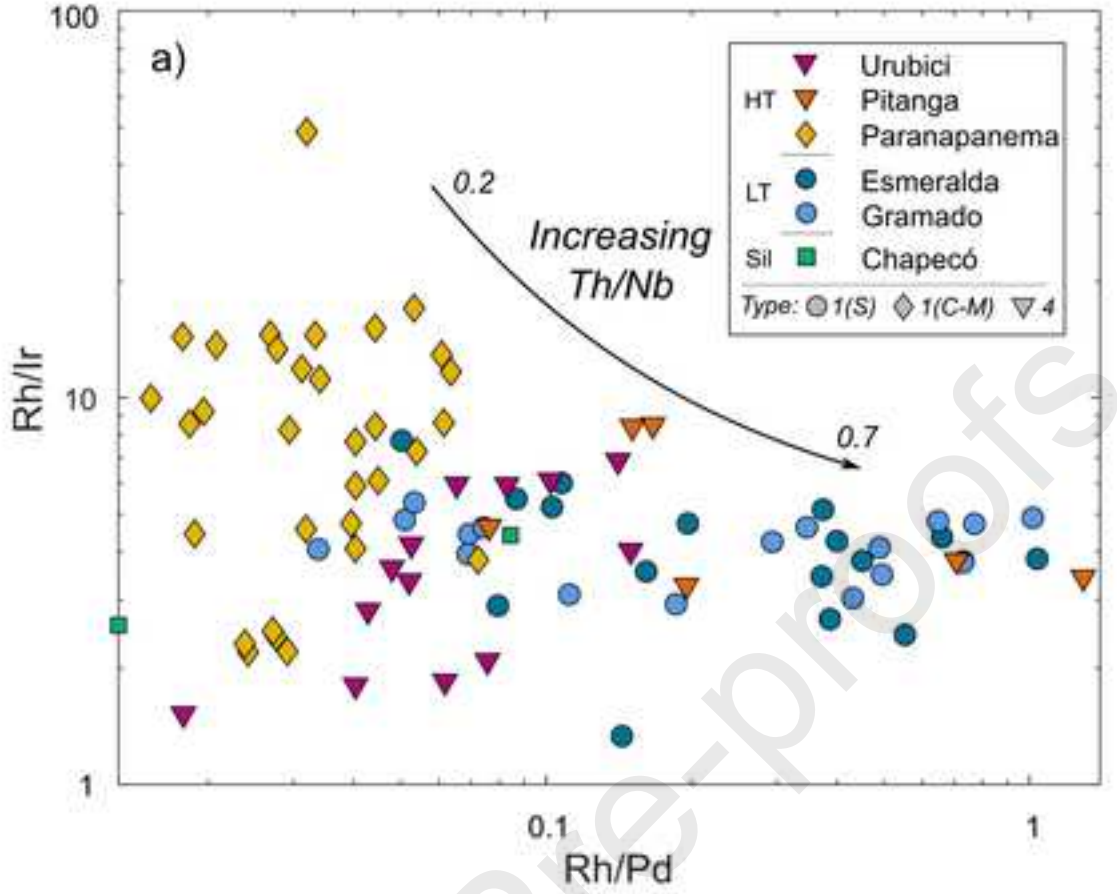

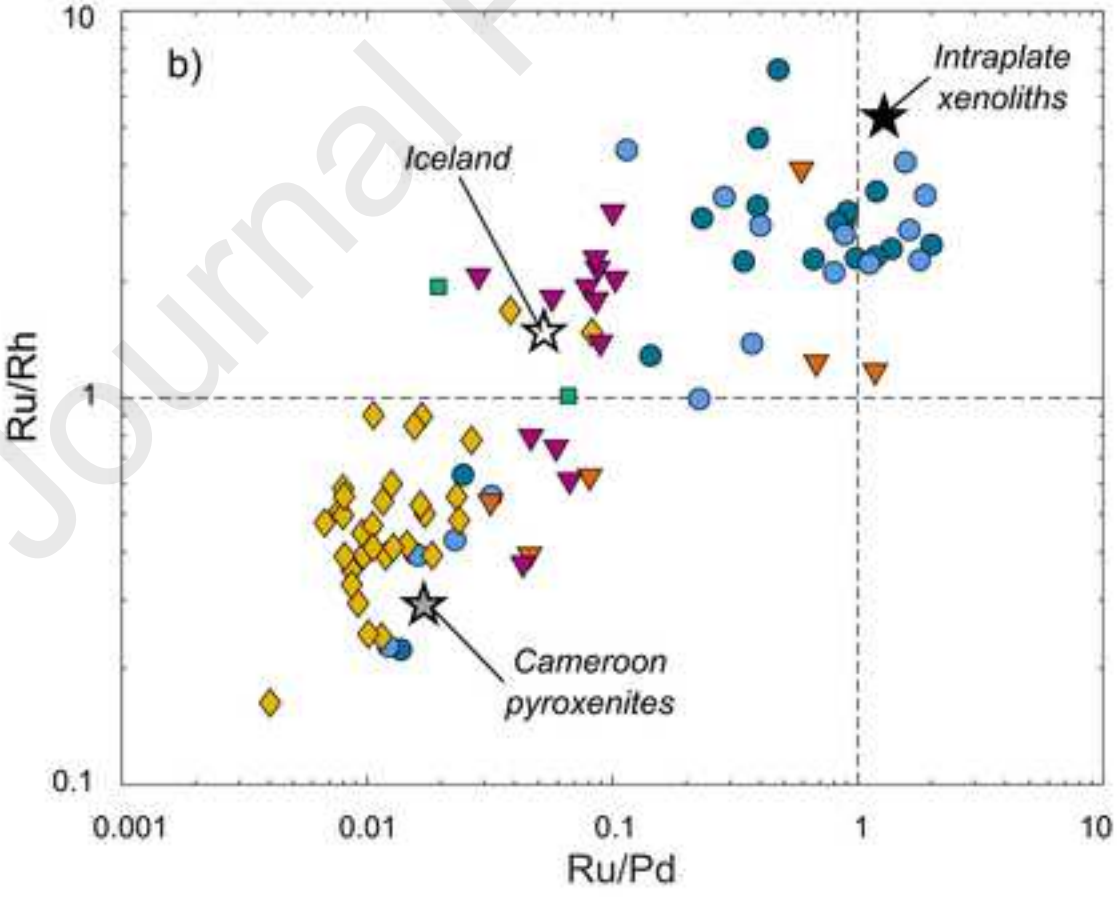

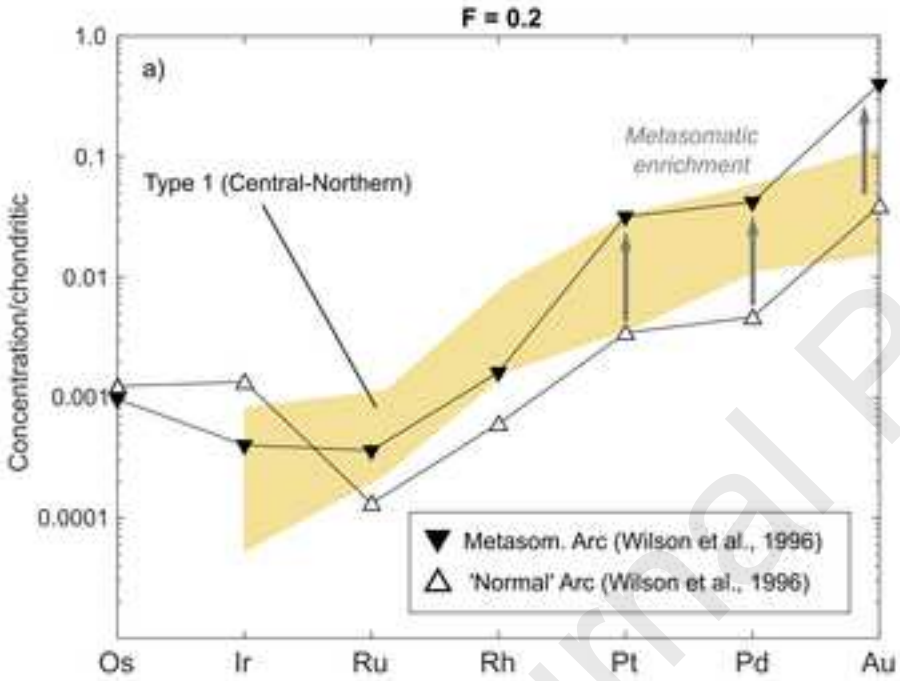

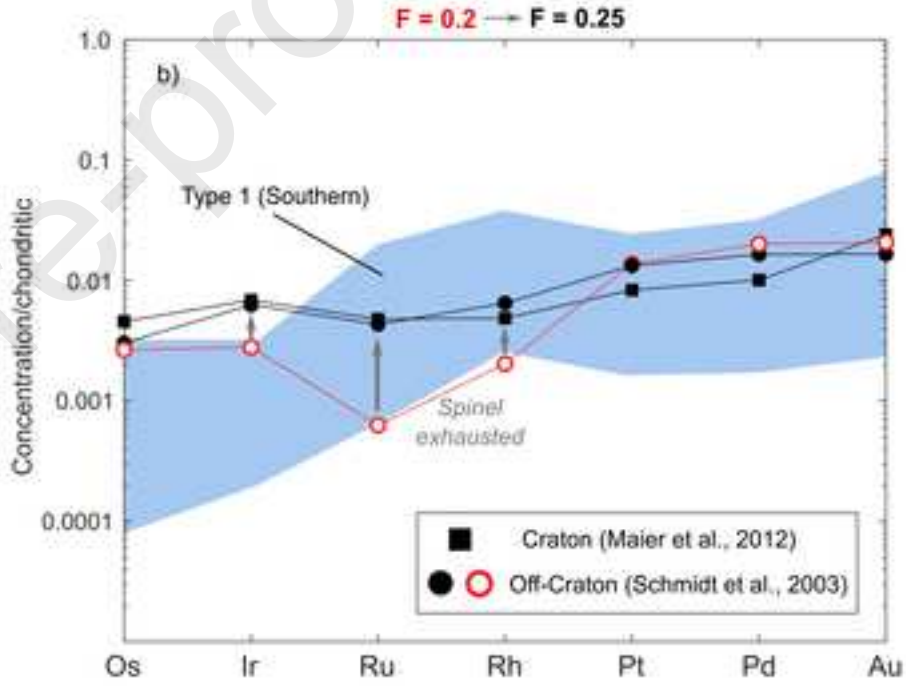

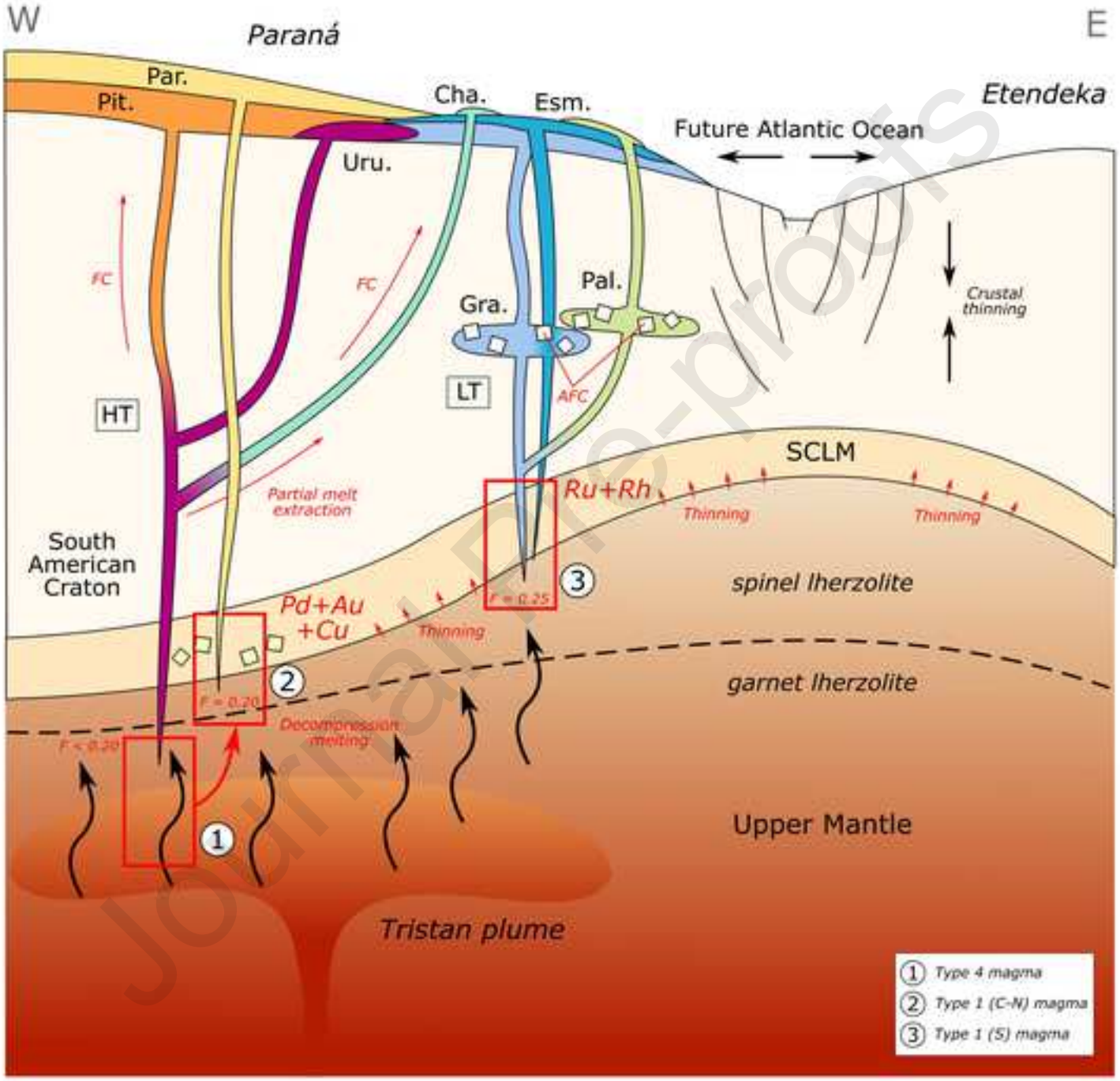

Peate et al. (1992)	Licht (2018)	Proportion	SiO_2 (wt%)	Zr (ppm)	TiO_2 (wt%)	P_2O_5 (wt%)
Gra, Esm, Par	Type 1 (S and C-N)	49.94%	<62.02	<522.15	<2.85	<0.413
-	Type 2	1.94%				>0.413
-	Type 3	3.85%			>2.85	<0.413
Pitanga, Urubici	Type 4	22.48%				>0.413
-	Type 5	0.06%		>522.15	<2.85	<0.413
-	Type 6	0.03%				>0.413
-	Type 7	0.03%			>2.85	<0.413
-	Type 8	-				>0.413
Palmas	Type 9	15.59%	>62.02	<522.15	<2.85	<0.413
-	Type 10	0.42%				>0.413
-	Type 11	0.03%			>2.85	<0.413
-	Type 12	0.03%				>0.413
-	Type 13	2.79%		>522.15	<2.85	<0.413
Chapecó	Type 14	3.79%				>0.413
-	Type 15	0			>2.85	<0.413
-	Type 16	0				>0.413

Setting	Mode (X)[a]	Melt Mode (p)[a]
Arc		
Olivine	0.52	-0.06
Opx	0.27	0.28
Cpx	0.17	0.62
Spinel	0.03	0.11
Sulphide	0.01	0.05
Craton		
Olivine	0.52	-0.06
Opx	0.27	0.28
Cpx	0.17	0.62
Spinel	0.03	0.12
Sulphide	0.01	0.04

Element	D olivine/liq[b]	D opx/liq[c]	D cpx/liq[d]	D spinel/liq[e]	D sulphide/liq[f]
Co	2.28	3	1.3	5	230
Ni	7.21	5	2.6	10	500
Cu	0.14	0.09	0.23	0.77	1470
Os	1.2	*0.05*	0.01	30	740000
Ir	0.77	*0.4*	*0.5*	132	458000
Ru	0.23	*3*	4.27	871	415000
Rh	1.94	*0.2*	0.25	400	205000
Pt	0.009	*1*	1.5	0.1	317000
Pd	0.12	*0.1*	*0.1*	0.14	190000
Au	0.12	*0.01*	*0.01*	0.076	10000

Source (C0)	Meta. Arc[g]	Normal Arc[g]	Craton[h]	Off-Craton[i]
Co (ppm)	80	100	100	108
Ni (ppm)	810	1980	2159	2240
Cu (ppm)	168	30	16.7	6.1
Os (ppb)	0.49	0.76	2	1.43
Ir (ppb)	0.31	1.26	2.33	2.3
Ru (ppb)	2	0.82	3.369932	3.43
Rh (ppb)	0.9	0.41	0.840309	1.21
Pt (ppb)	14.96	1.97	3.891727	6.91
Pd (ppb)	6.42	0.86	1.857811	3.28
Au (ppb)	14.3	1.69	1.06642	0.79